

Introduction to the statistical methodology for brain connectivity analysis

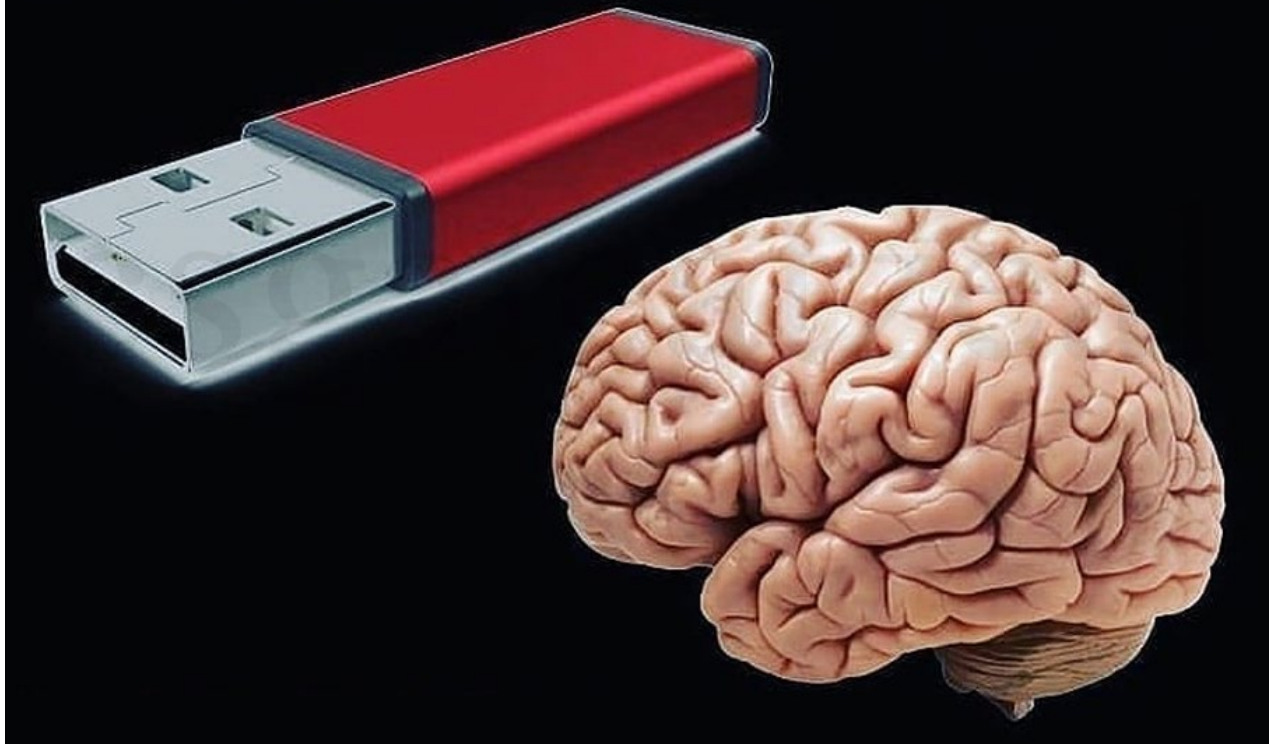
Jose M. Sanchez Bornot

University of Ulster, Magee Campus,
Intelligent Systems Research Centre



“More important than knowing something is to know how and where to search for it.”

The Human brain has an estimated storage capacity of 256 exabytes (or 256 billion GB) the equivalent of 1.2 billion average PC hard drives.



OUTLINE

Generative models

Matlab, Simulations and Methods

- MVAR
- Linear model
- Granger causality
- State-space model
- Hemodynamic (DCM) model

Brain anatomical connectivity

Resting-state functional connectivity (MRI, fMRI, PET)

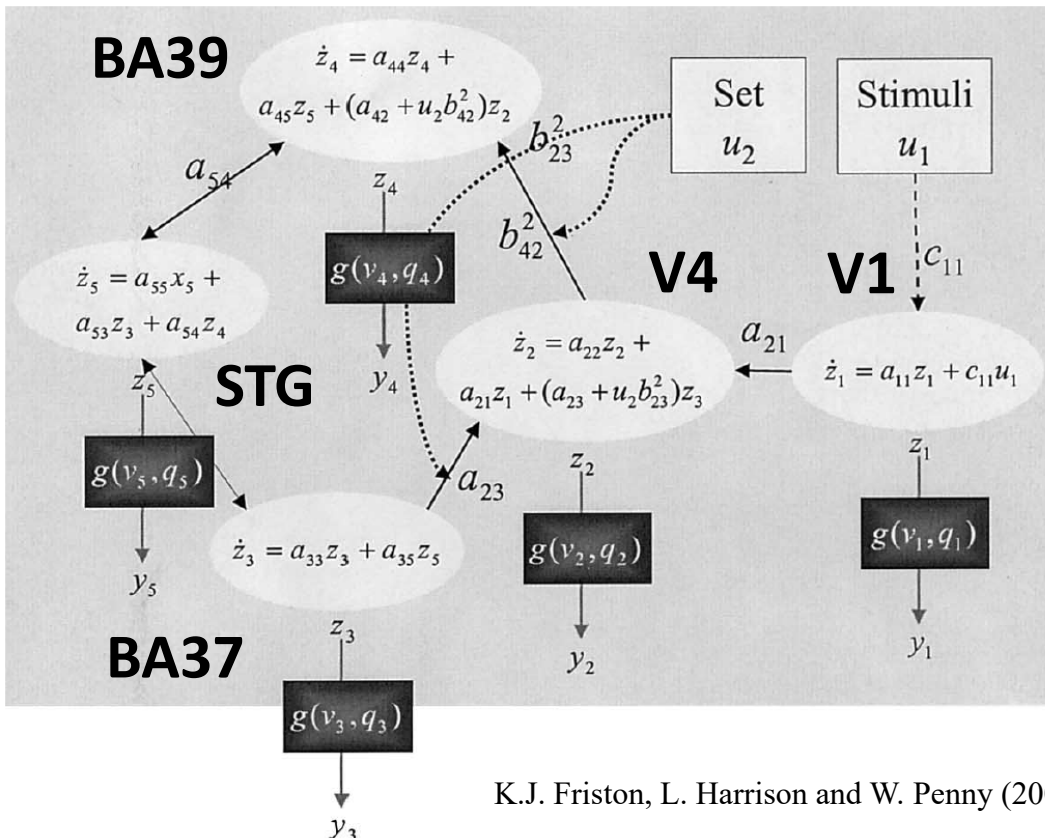
- Seed-based correlation and ICA (default-mode networks)
- General considerations

EEG/MEG-based functional connectivity

- Sensor vs source-based functional connectivity
- The importance of inverse solutions
- Practical considerations

Generative models

Multivariate autoregressive
(MVAR) model: $\mathbf{Y} = \mathbf{XB} + \mathbf{E}$



Example: Bivariate VAR(2) Model

$$\begin{bmatrix} y_{1t} \\ y_{2t} \end{bmatrix} = \begin{bmatrix} a_1 \\ a_2 \end{bmatrix} + \begin{bmatrix} b_{11}^1 & b_{12}^1 \\ b_{21}^1 & b_{22}^1 \end{bmatrix} \begin{bmatrix} y_{1t-1} \\ y_{2t-1} \end{bmatrix} + \begin{bmatrix} b_{11}^2 & b_{12}^2 \\ b_{21}^2 & b_{22}^2 \end{bmatrix} \begin{bmatrix} y_{1t-2} \\ y_{2t-2} \end{bmatrix} + \begin{bmatrix} \varepsilon_{1t} \\ \varepsilon_{2t} \end{bmatrix}$$

Or:

$$y_{1t} = a_1 + b_{11}^1 y_{1t-1} + b_{12}^1 y_{2t-1} + b_{11}^2 y_{1t-2} + b_{12}^2 y_{2t-2} + \varepsilon_{1t}$$
$$y_{2t} = a_2 + b_{21}^1 y_{1t-1} + b_{22}^1 y_{2t-1} + b_{21}^2 y_{1t-2} + b_{22}^2 y_{2t-2} + \varepsilon_{2t}$$

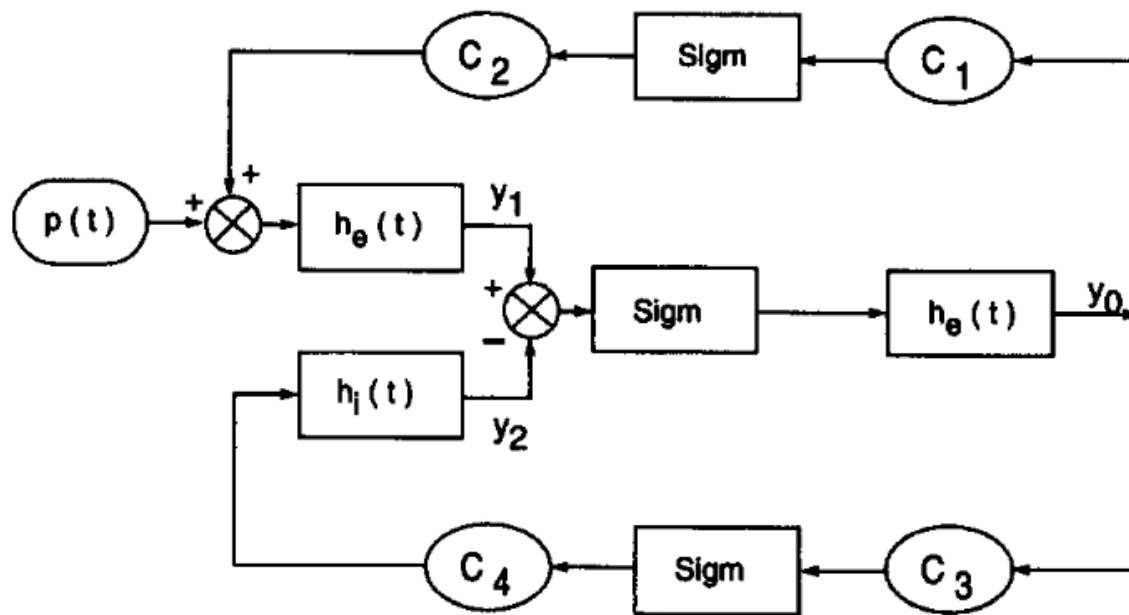
<https://medium.com/analytics-vidhya/introduction-to-vector-autoregression-6ec386db387e>

Dynamical systems (e.g., DCM):

$$\frac{d\mathbf{z}}{dt} = \left(\mathbf{A} + \sum_{j=1}^m u_j \mathbf{B}^{(j)} \right) \mathbf{z} + \mathbf{C}\mathbf{u}$$

Jansen-Rit model

Jansen, B.H. and Rit, V.G., 1995. Electroencephalogram and visual evoked potential generation in a mathematical model of coupled cortical columns. *Biological cybernetics*, 73(4), pp.357-366



The cortical column is modelled by a population of 'feedforward' pyramidal cells, receiving inhibitory and excitatory feedback from local interneurons (other pyramidal, stellate or basket cells residing in the same column) and excitatory input from neighbouring or more distant columns . The latter input is represented by a pulse density $p(t)$ which can be any arbitrary function, including white noise.

$$\dot{y}_0(t) = y_3(t)$$

$$\dot{y}_3(t) = Aa \operatorname{Sigm}[y_1(t) - y_2(t)] - 2ay_3(t) - a^2 y_0(t)$$

$$\dot{y}_1(t) = y_4(t)$$

$$\begin{aligned} \dot{y}_4(t) = & Aa\{p(t) + C_2 \operatorname{Sigm}[C_1 y_0(t)]\} \\ & - 2ay_4(t) - a^2 y_1(t) \end{aligned}$$

$$\dot{y}_2(t) = y_5(t)$$

$$\dot{y}_5(t) = Bb\{C_4 \operatorname{Sigm}[C_3 y_0(t)]\} - 2by_5(t) - b^2 y_2(t)$$

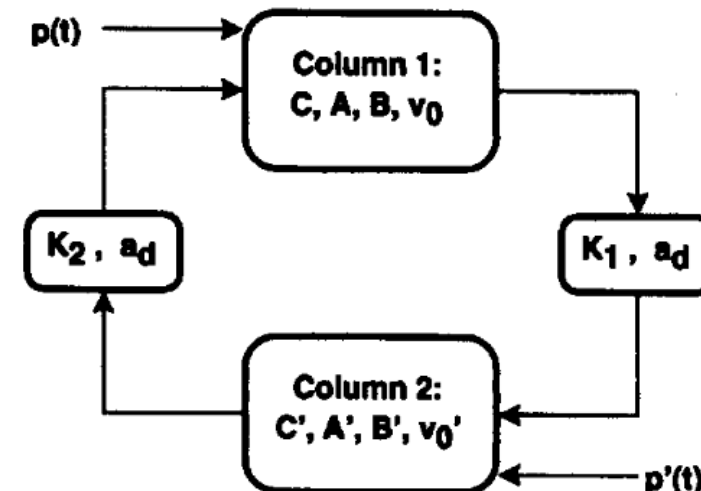


Fig. 2. Schematic diagram of the double-column model

Hodgkin-Huxley equations

$$\begin{aligned} C \dot{V} &= I - \overbrace{\bar{g}_K n^4 (V - E_K)}^{I_K} - \overbrace{\bar{g}_{Na} m^3 h (V - E_{Na})}^{I_{Na}} - \overbrace{g_L (V - E_L)}^{I_L} \\ \dot{n} &= \alpha_n(V)(1 - n) - \beta_n(V)n \\ \dot{m} &= \alpha_m(V)(1 - m) - \beta_m(V)m \\ \dot{h} &= \alpha_h(V)(1 - h) - \beta_h(V)h , \end{aligned}$$

Izhikevich, E.M., 2007. *Dynamical systems in neuroscience*. MIT press.

C : membrane capacitance.

V : membrane voltage.

I : applied current.

I_L : Ohmic leak current, mostly driven by flux of Cl^- ions.

$\alpha(\cdot), \beta(\cdot)$: voltage-dependent functions for the transition rate between open/closed states of the ion channels.

n : activation variable for K^+ flux (4 gates).

m : activation variable for Na^+ flux (3 gates).

h : inactivation variable for Na^+ flux (1 gate).

Typical values of maximal conductance are:

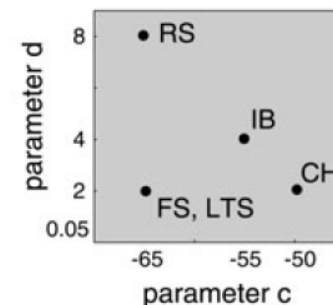
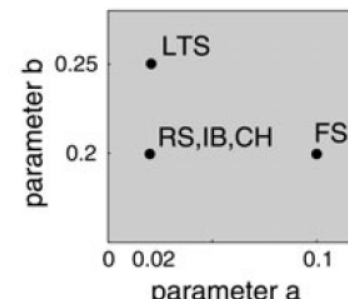
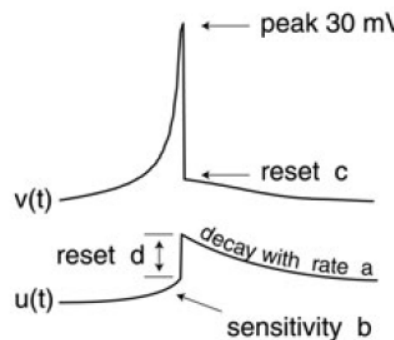
$$\bar{g}_K = 36 \text{ mS/cm}^2 \quad \bar{g}_{Na} = 120 \text{ mS/cm}^2 , \quad g_L = 0.3 \text{ mS/cm}^2 .$$

Izhikevich's spiking neuronal network model

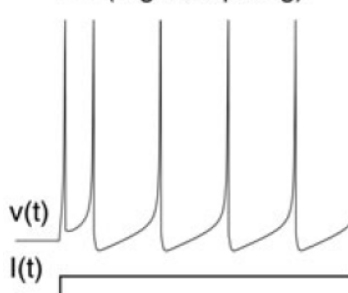
$$\dot{v} = 0.04v^2 + 5v + 140 - u - I_{\text{syn}}$$

$$\dot{u} = a(bv - u)$$

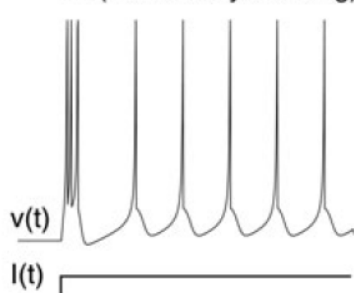
if $v(t) = 30$ mV, then $\begin{cases} v \leftarrow c \\ u \leftarrow u + d \end{cases}$



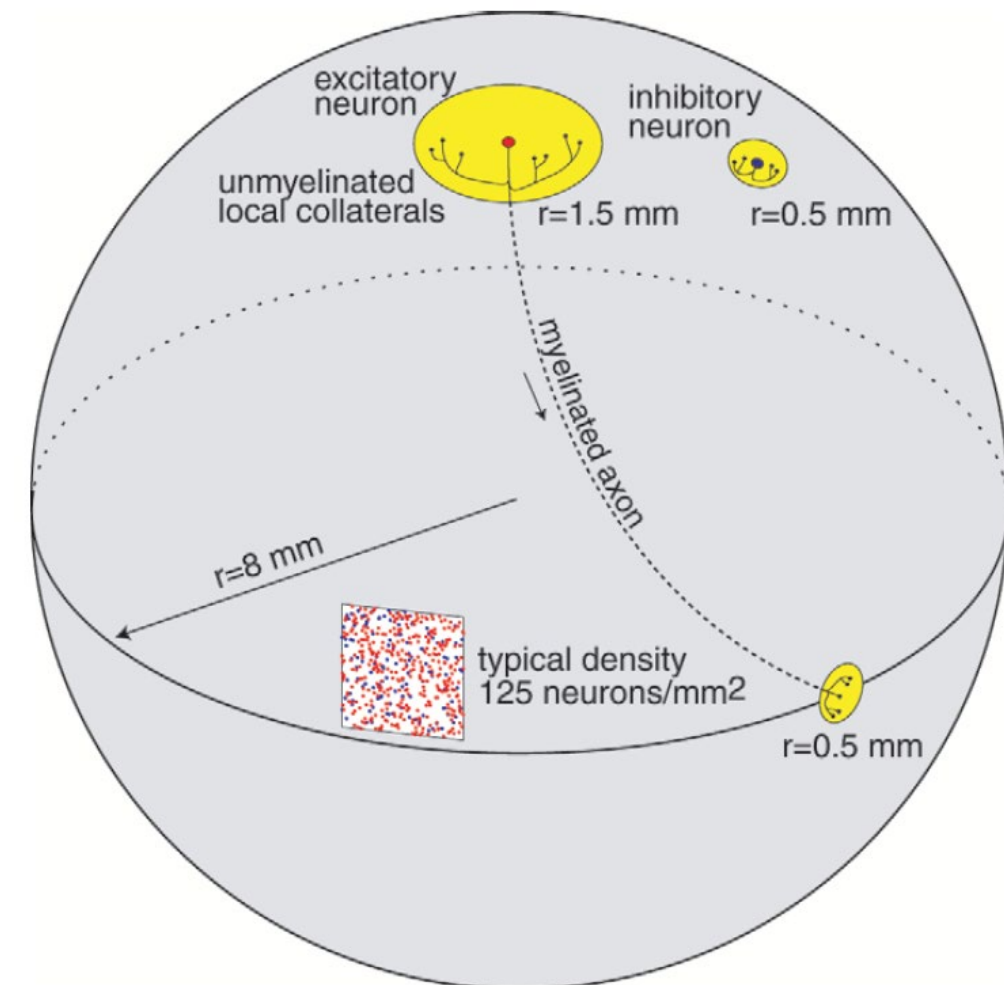
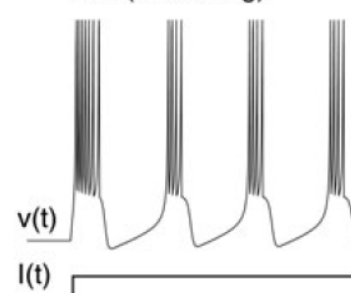
RS (regular spiking)



IB (intrinsically bursting)



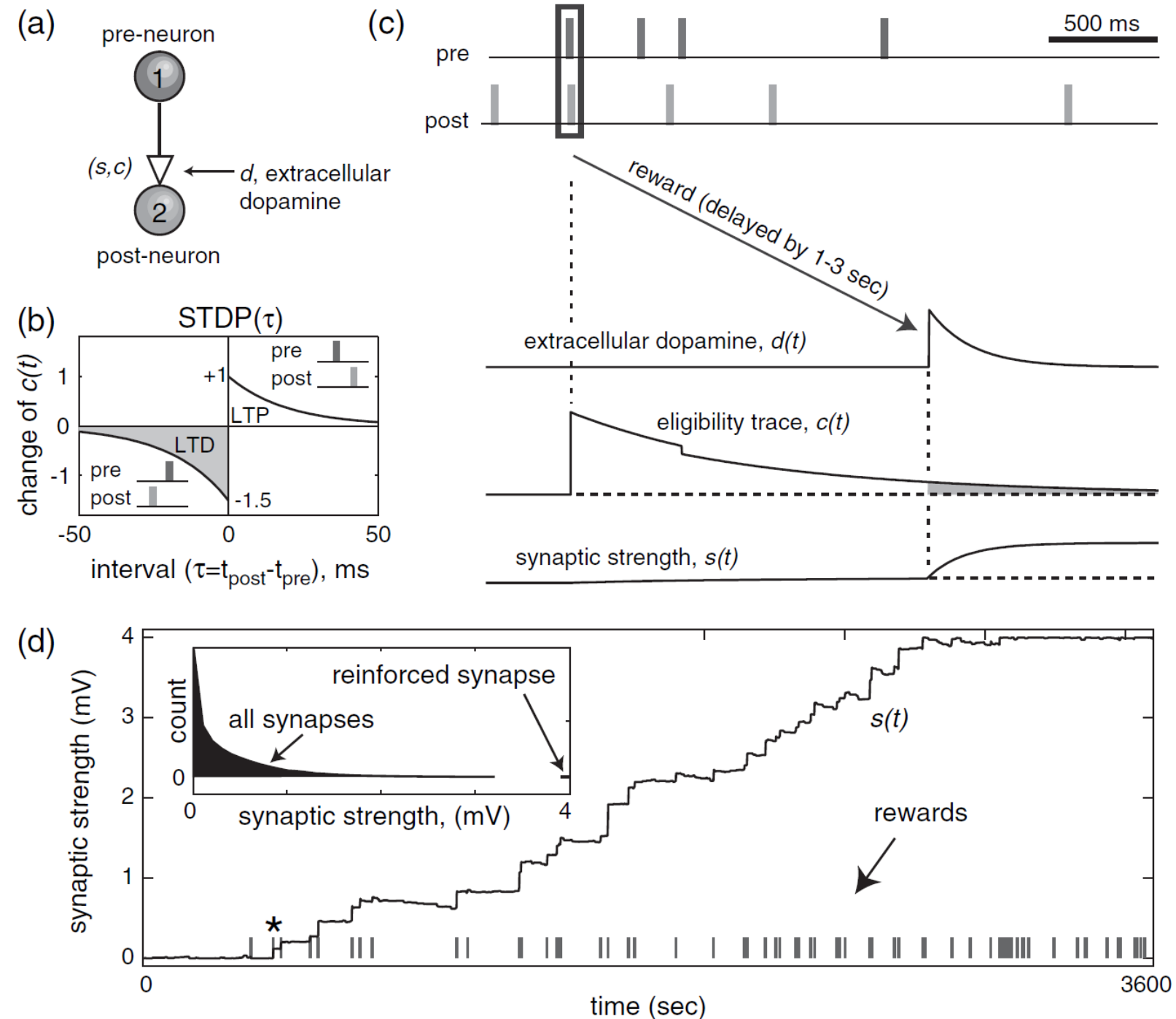
CH (chattering)



Izhikevich, E.M., Gally, J.A. and Edelman, G.M., 2004. Spike-timing dynamics of neuronal groups. *Cerebral cortex*, 14(8), pp.933-944.

Izhikevich: Solving the Distal Reward Problem through Linkage of STDP and Dopamine Signaling. Cerebral Cortex, 2007.

Figure 1. Instrumental conditioning of a synapse. (a) The dynamics of each synapse is described by 2 phenomenological variables governed by equations (1) and (2): synapse strength s and eligibility trace c , which are gated by the extracellular DA d . Firings of the pre- and postsynaptic neurons induce changes to the variable c according to the STDP rule (shown in b). These changes result in modification of the synaptic strength, s , only when extracellular DA is present ($d>0$) during the critical window of a few seconds while the eligibility trace c decays to zero. (c) The magnification of the region in (d) marked by *. To reinforce coincident firings of 2 coupled neurons, we deliver a reward (step-increase of variable d) with a random delay (between 1 and 3 s) each time a postsynaptic firing occurs within 10 ms after a presynaptic firing (marked by a rectangle in c). This rare event increases c greater than any random firings of the same neurons during the delayed period. (d) Consistent rewarding of each such event results in the gradual increase of synaptic strength, s , which increases the probability of coincident firings and brings even more reward. The time course of a typical unreinforced synapse (not shown here) looks like a random walk near 0. The inset shows the distribution of all synaptic weights in the network. The reinforced synapse is potentiated to the maximal allowable value 4 mV (42 out of 50 experiments) whereas the other synapses are not.



Large-scale model of mammalian thalamocortical systems

Eugene M. Izhikevich and Gerald M. Edelman*

The Neurosciences Institute, 10640 John Jay Hopkins Drive, San Diego, CA 92121

Contributed by Gerald M. Edelman, December 27, 2007 (sent for review December 21, 2007)

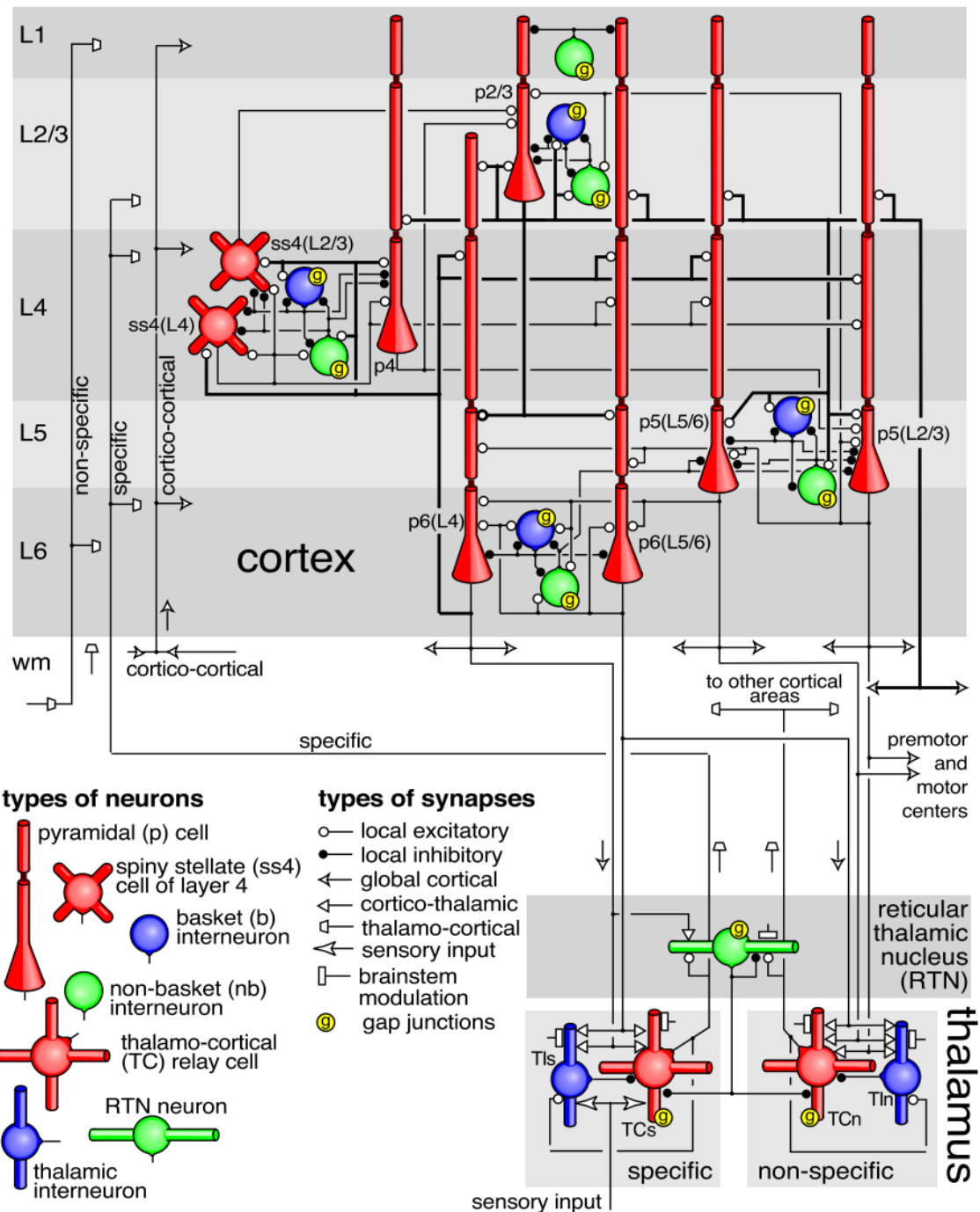
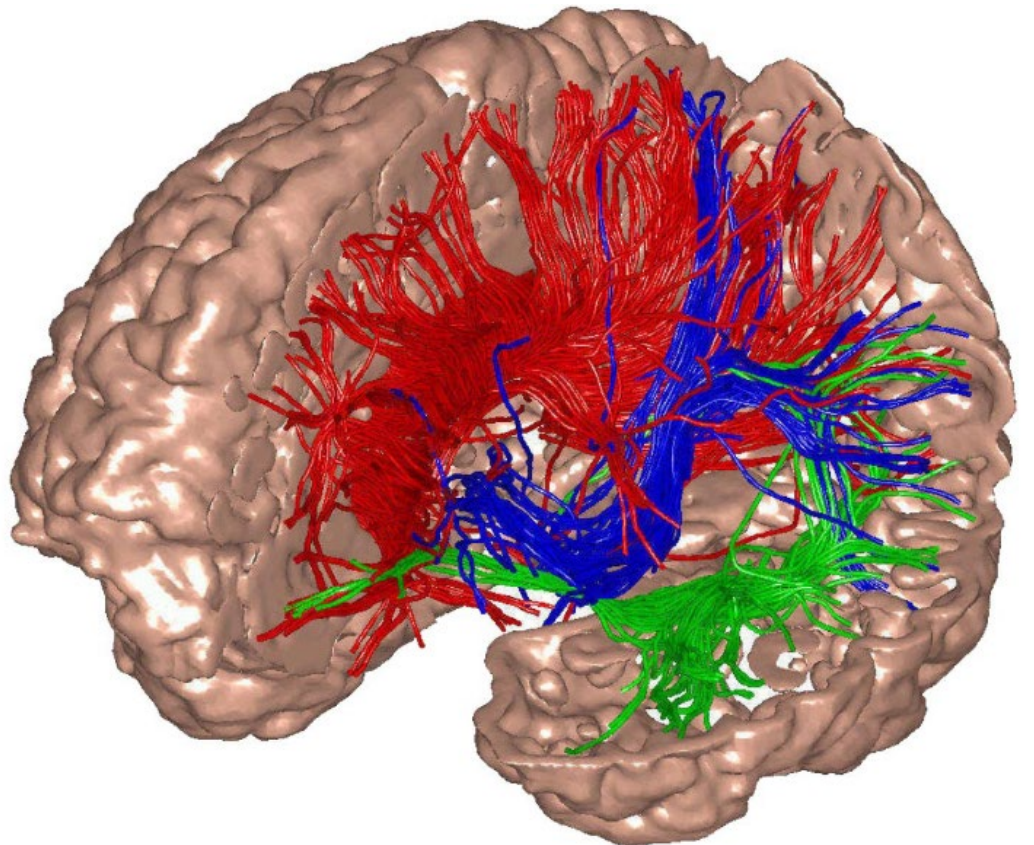


Figure 9 (Izhikevich):
Distribution of neuronal types and synapses in the model.

Each row represents a single postsynaptic neuron of a certain type.

Multiple compartments, if they exist, are indicated.

Each element in a row represents the percentage of synapses of a particular type to that neuron.

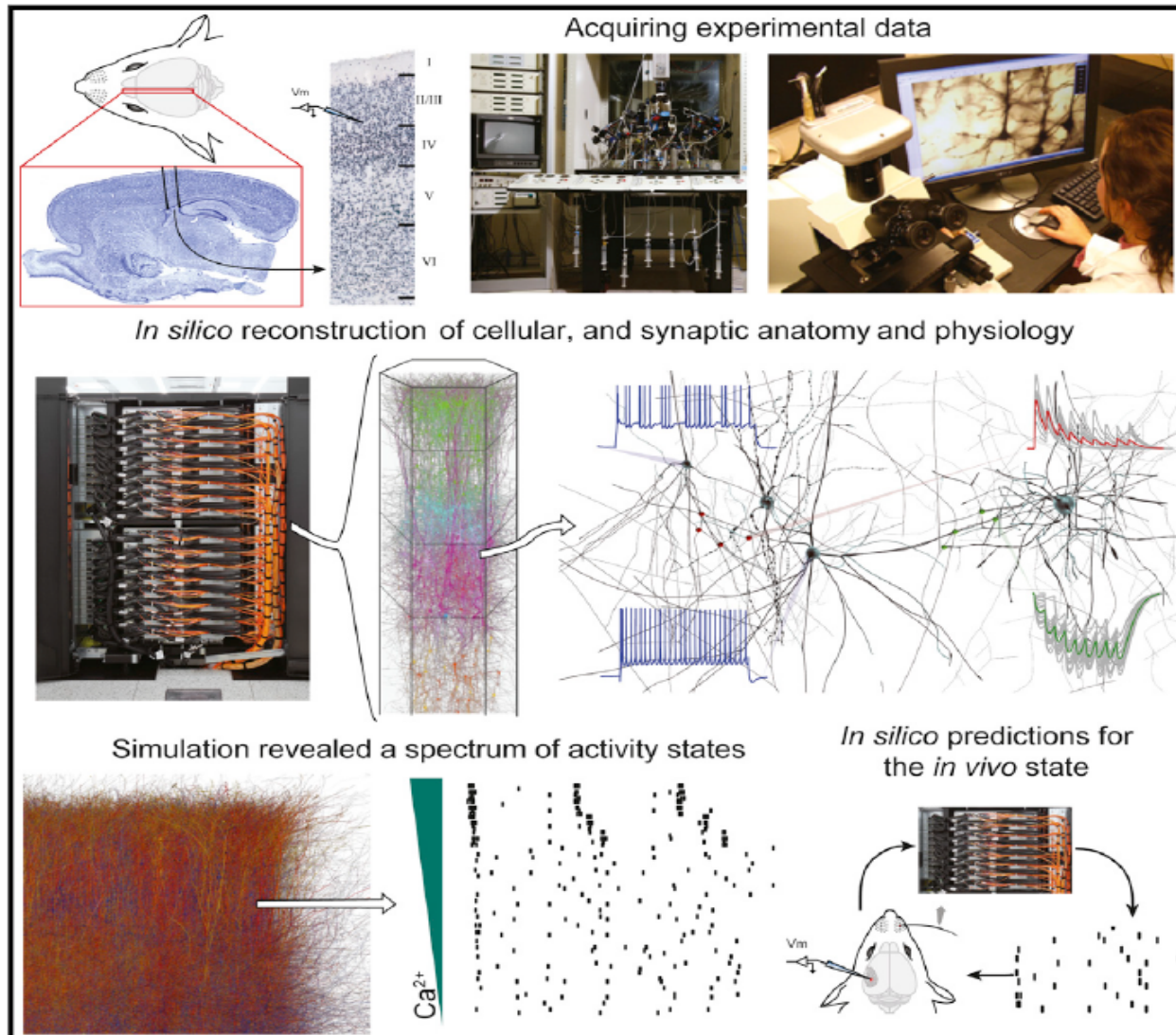
The most significant connections are shown in Fig. 8.

Shaded regions denote plastic connections.

postsynaptic neurons	percent of cells		number of synapses		corticocortical																			
	nb1	p2/3	b2/3	nb2/3	ss4(L4)	ss4(L2/3)	p4	b4	nb4	p5(L2/3)	p5(L5/6)	b5	nb5	p6(L4)	p6(L5/6)	b6	nb6	Tcs	Tcn	Tls	Tln	TRN		
	nb1	p2/3 L2/3	L1	b2/3	ss4(L4)	ss4(L2/3)	p4	b4	nb4	p5(L2/3)	p5(L5/6)	b5	nb5	p6(L4)	p6(L5/6)	b6	nb6	Tcs	Tcn	Tls	Tln	TRN		
nb1	1.5	8890	10.1	6.3	0.6	1.1	.	.	0.1	0.1	.	.	77.6	.	4.1		
p2/3 L2/3	26	5800	.	59.9	9.1	4.4	0.6	6.9	7.7	.	0.8	7.4	.	.	0.8	.	78	.	4.1	.	.	.		
L1	1306	10.2	6.3	0.1	1.1	.	.	0.1	.	.	.	0.1	78	.	4.1	.	.	.		
b2/3	3.1	3854	1.3	51.6	10.6	3.4	0.5	5.8	6.6	.	0.8	6.3	.	.	2.1	.	0.7	9.8	.	0.5	.	.	.	
nb2/3	4.2	3307	1.7	48.6	11.4	3.3	0.5	5.5	6.2	.	0.8	5.9	.	.	1.8	.	0.6	13	.	0.7	.	.	.	
ss4(L4)	9.2	5792	.	2.7	0.2	0.6	11.9	3.7	4.1	7.1	2	0.8	0.1	.	32.7	.	5.8	25.3	1.7	1.3	.	.	.	
ss4(L2/3)	9.2	4989	.	5.6	0.4	0.8	11.3	3.8	4.3	7.2	2.1	1.1	0.1	.	31.1	.	5.5	23.9	1.7	1.3	.	.	.	
p4 L4	9.2	5031	.	4.3	0.2	0.6	11.5	3.6	4.2	7.2	2.1	1.2	0.1	.	31.4	0.1	5.9	24.5	1.7	1.3	.	.	.	
L2/3	866	.	63.1	5.1	4.1	0.6	7.2	8.1	.	0.6	7.8	.	.	2.5	.	0.8	
L1	806	10.2	6.3	0.1	1.1	.	.	0.1	.	.	0.1	78	.	4.1	
b4	5.4	3230	.	5.8	0.5	0.8	11	3.8	4.2	8.4	2.4	1.1	.	.	30.3	.	5.4	23.3	1.6	1.2	.	.	.	
nb4	1.5	3688	.	2.7	0.2	0.6	11.7	3.6	4	8.2	2.3	0.8	0.1	.	32.2	.	5.7	24.9	1.7	1.3	.	.	.	
p5(L2/3) L5	4.8	4316	.	45.9	1.8	0.3	3.3	2	7.5	.	0.9	11.7	1	0.8	1.1	2.3	2.1	.	11.5	7.2	0.1	0.4	.	.
L4	283	.	2.8	0.1	0.7	12.2	3.8	4.2	5.2	1.5	0.8	0.1	.	.	33.7	.	5.9	26	1.8	1.4	.	.	.	
L2/3	412	.	63.1	5.1	4.1	0.6	7.2	8.1	.	0.6	7.8	.	.	2.5	.	0.8	
L1	185	10.2	6.3	0.1	1.1	.	.	0.1	.	.	0.1	78	.	4.1	
p5(L5/6) L5	1.3	5101	.	44.3	1.7	0.2	3.2	2	7.3	.	0.8	11.3	1.2	0.8	1.1	2.3	2.5	0.3	11.3	9.2	0.2	0.5	.	.
L4	949	.	2.8	0.1	0.7	12.2	3.8	4.2	5.2	1.5	0.8	0.1	.	.	33.7	.	5.9	26	1.8	1.4	.	.	.	
L2/3	1367	.	63.1	5.1	4.1	0.6	7.2	8.1	.	0.6	7.8	.	.	2.5	.	0.8	
L1	5658	10.2	6.3	0.1	1.1	.	.	0.1	.	.	0.1	78	.	4.1	
b5	0.6	2981	.	45.5	2.3	0.2	3.3	2	7.5	.	1.1	11.6	1	0.9	1.3	2.3	2	.	11.4	7.2	0.1	0.4	.	.
nb5	0.8	2981	.	45.5	2.3	0.2	3.3	2	7.5	.	1.1	11.6	1	0.9	1.3	2.3	2	.	11.4	7.2	0.1	0.4	.	.
p6(L4) L6	13.6	3261	.	2.5	0.1	0.1	0.7	0.9	1.3	.	0.1	0.1	4.9	.	0.3	1.2	13.2	7.7	7.7	55.7	0.6	2.9	.	.
L5	1066	.	46.8	0.8	0.3	3.4	2.1	7.7	.	0.6	11.9	1	0.6	0.8	2.3	2.1	.	11.7	7.4	0.1	0.4	.	.	
L4	1915	.	2.8	0.1	0.7	12.2	3.8	4.2	5.2	1.5	0.8	0.1	.	.	33.7	.	5.9	26	1.8	1.4	.	.	.	
L2/3	121	.	63.1	5.1	4.1	0.6	7.2	8.1	.	0.6	7.8	.	.	2.5	.	0.8	
p6(L5/6) L6	4.5	5573	.	2.5	0.1	0.1	0.7	0.9	1.3	.	0.1	0.1	4.9	.	0.3	1.2	13.2	7.8	7.8	55.7	0.6	2.9	.	.
L5	257	.	46.8	0.8	0.3	3.4	2.1	7.7	.	0.6	11.9	1	0.6	0.8	2.3	2.1	.	11.7	7.4	0.1	0.4	.	.	
L4	243	.	2.8	0.1	0.7	12.2	3.8	4.2	5.2	1.5	0.8	0.1	.	.	33.7	.	5.9	26	1.8	1.4	.	.	.	
L2/3	286	.	63.1	5.1	4.1	0.6	7.2	8.1	.	0.6	7.8	.	.	2.5	.	0.8	
L1	62	10.2	6.3	0.1	1.1	.	.	0.1	.	.	0.1	78	.	4.1	
b6	2	3220	.	2.5	0.1	0.1	0.7	0.9	1.3	.	0.1	0.1	4.9	.	0.4	1.2	13.2	7.7	7.7	55.7	0.6	2.9	.	.
nb6	2	3220	.	2.5	0.1	0.1	0.7	0.9	1.3	.	0.1	0.1	4.9	.	0.4	1.2	13.2	7.7	7.7	55.7	0.6	2.9	.	.
brainstem sensory																								
Tcs	0.5	4000	31	.	7.1	23	8	5	.	25.9
Tcn	0.5	4000	31	.	7.1	14	3.8	.	.	13.2	5	.	25.9
Tls	0.1	3000	13.5	.	48.7	9.8	3.3	0.4	24.4	.	.
Tln	0.1	3000	13.4	.	48.7	5.8	1.6	.	.	5.4	0.6	24.4	.	.
TRN	0.5	4000	40	30	10	10	.	10

Reconstruction and Simulation of Neocortical Microcircuitry

Graphical Abstract



Authors

Henry Markram, Eilif Müller,
Srikanth Ramaswamy,
Michael W. Reimann, ..., Javier DeFelipe,
Sean L. Hill, Idan Segev, Felix Schürmann

Correspondence

henry.markram@epfl.ch

In Brief

A digital reconstruction and simulation of the anatomy and physiology of neocortical microcircuitry reproduces an array of *in vitro* and *in vivo* experiments without parameter tuning and suggests that cellular and synaptic mechanisms can dynamically reconfigure the state of the network to support diverse information processing strategies.

Matlab, Simulations and Methods

Overview of Matlab's notation with code examples

Diagonal matrix

```
>> A = diag([1 3 5])
```

A =

1	0	0
0	3	0
0	0	5

Matrix of random uniform numbers: dim=3x4

```
>> B = rand(3,4)
```

B =

0.0975	0.9575	0.9706	0.8003
0.2785	0.9649	0.9572	0.1419
0.5469	0.1576	0.4854	0.4218

3D matrix of random numbers with Gaussian (normal) distributions

```
>> D = randn(4,3,2)
```

D(:,:,1) =

1.4897	-1.2075	1.0347
1.4090	0.7172	0.7269
1.4172	1.6302	-0.3034
0.6715	0.4889	0.2939

D(:,:,2) =

-0.7873	-0.8095	-0.7549
0.8884	-2.9443	1.3703
-1.1471	1.4384	-1.7115
-1.0689	0.3252	-0.1022

D(:,:,2) =

-0.7873	-0.8095	-0.7549
---------	---------	---------

D(:,:,1) =

1.3703		
1.4897	-1.2075	1.0347
1.4090	0.7172	0.7269
1.4172	1.6302	-0.3034
0.6715	0.4889	0.2939

Left-side multiplication with a diagonal matrix

```
>> C = A*B
```

C =

0.0975	0.9575	0.9706	0.8003
0.8355	2.8947	2.8715	0.4257
2.7344	0.7881	2.4269	2.1088

Friendly functions: reshape, repmat

```
>> E = reshape(D, [4 2 3])
```

E(:,:,1) =

1.4897	-1.2075
1.4090	0.7172
1.4172	1.6302
0.6715	0.4889

E(:,:,2) =

1.0347	-0.7873
0.7269	0.8884
-0.3034	-1.1471
0.2939	-1.0689

E(:,:,3) =

-0.8095	-0.7549
-2.9443	1.3703
1.4384	-1.7115
0.3252	-0.1022

```
>> repmat('ABC', [2 3])  
'ABCABCABC'  
'ABCABCABC'
```

Colon (:) operations and indexing

```
>> C(1,:)
```

0.0975	0.9575	0.9706	0.8003
--------	--------	--------	--------

```
>> C(:,2)
```

```
>> [C(2:end,2:end); [3 4 5]]
```

0.9575	2.8947	2.8715	0.4257
--------	--------	--------	--------

2.8947	0.7881	2.4269	2.1088
--------	--------	--------	--------

0.7881	3.0000	4.0000	5.0000
--------	--------	--------	--------

```
>> ind = 11:-1:5
```

ind =

11	10	9	8	7	6	5
----	----	---	---	---	---	---

High-level operations such as for and while loops

```
>> f = zeros(1,7);
```

```
>> f(1:2) = 1;
```

```
>> for k = 3:length(f)
```

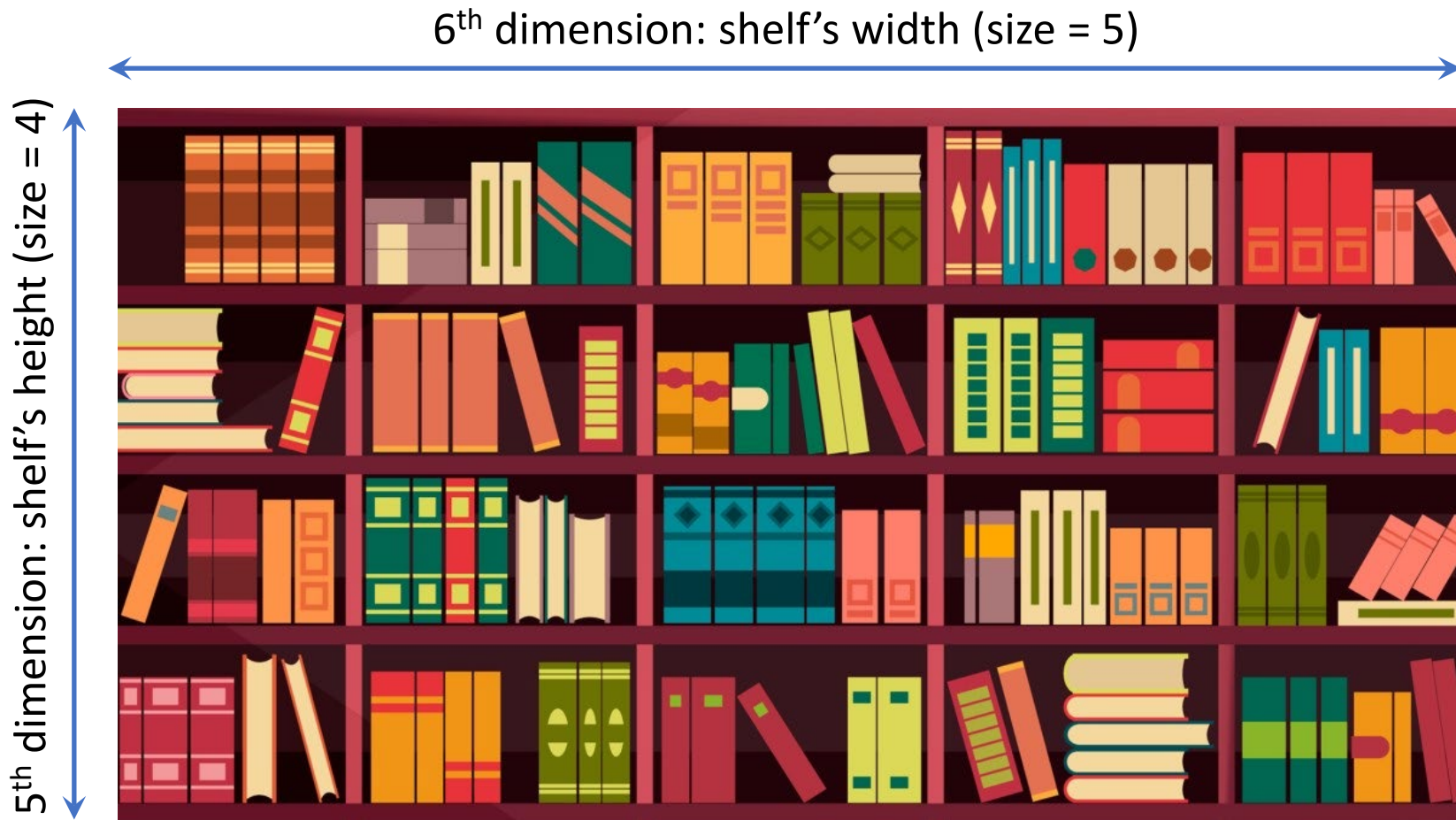
```
    f(k) = f(k-1) + f(k-2);
```

```
end
```

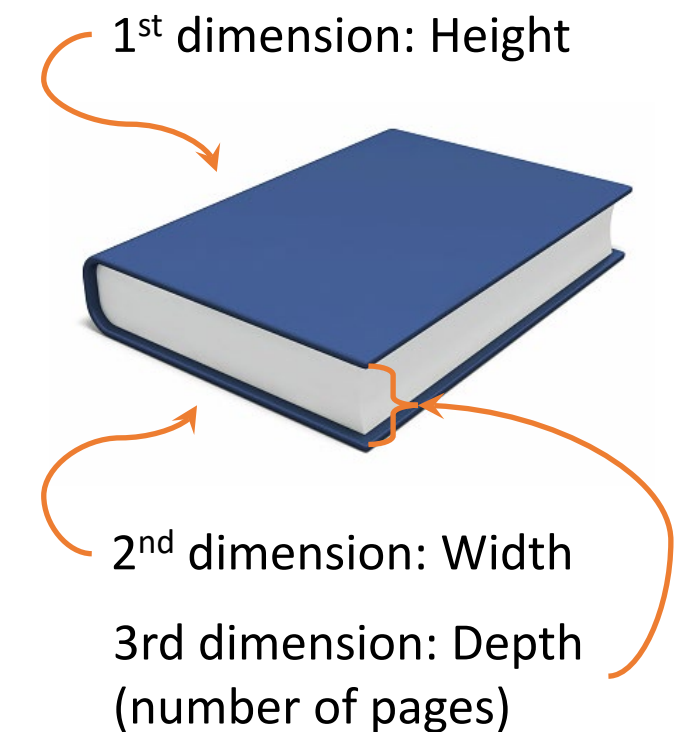
```
>> f
```

1	1	2	3	5	8	13
---	---	---	---	---	---	----

A six-dimensional matrix (assuming all books have same dimensions and shelf's spaces are equals)



<https://ncbiinsights.ncbi.nlm.nih.gov/2018/07/24/add-your-full-text-book-ncbi-bookshelf/>



Where is the 4th dimension?

Stokes, P.A. and Purdon, P.L., 2017. A study of problems encountered in Granger causality analysis from a neuroscience perspective.

```

Fs = 120; % sampling frequency is 120 Hz
T = 2*Fs; % 2 seconds simulation
r = [0.9 0.7 0.8];
f = [40 10 50];
dt = 1/Fs;
theta = 2*pi*f*dt;

N = 3; % number of nodes
p = 3; % true order of the MVAR model
A = zeros(N,N,p);
A(:,:,1) = diag(2*r.*cos(theta)) + [0 0 0; -0.356 0 0; 0 -0.3098 0];
A(:,:,2) = diag(-r.^2) + [0 0 0; 0.7136 0 0; 0 0.5 0];
A(:,:,3) = [0 0 0; -0.356 0 0; 0 -0.3098 0];

ss = 1; % space noise's standard deviation
x = ss*randn(N,T);
for t = p+1:T
    for k = 1:p
        x(:,t) = x(:,t) + A(:,:,k)*x(:,t-k);
    end
end

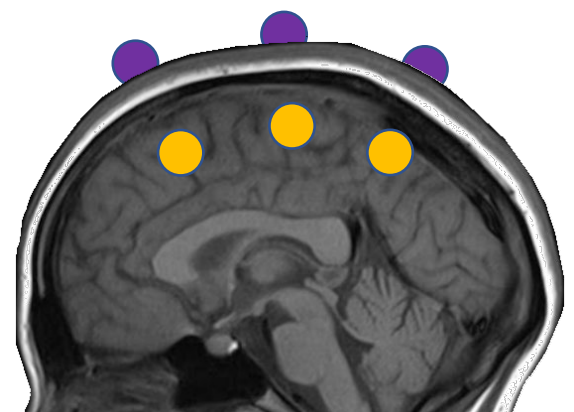
B = [1 0.5 0.2; 0.5 1 0.5; 0.2 0.5 1]; % mixing matrix
so = 1; % observation noise's standard deviation
y = B*x + so*randn(N,T);

figure;
subplot 211; plot(x'); title('x: hidden dynamics'); axis tight
subplot 212; plot(y'); title('y: observed dynamics'); axis tight

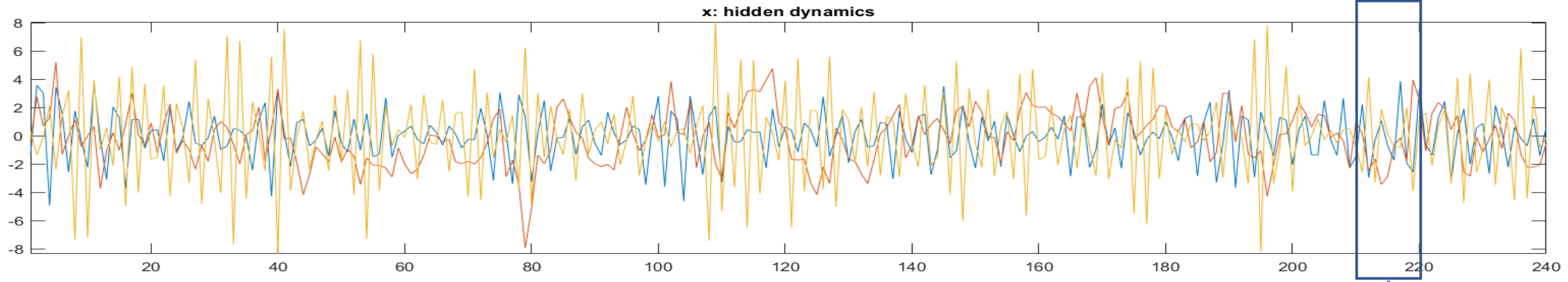
```

$$\begin{aligned}
\begin{bmatrix} x_{1,t} \\ x_{2,t} \\ x_{3,t} \end{bmatrix} &= \underbrace{\begin{bmatrix} 2r_1 \cos(\theta_1) & 0 & 0 \\ -0.356 & 2r_2 \cos(\theta_2) & 0 \\ 0 & -0.3098 & 2r_3 \cos(\theta_3) \end{bmatrix}}_{A_1} \begin{bmatrix} x_{1,t-1} \\ x_{2,t-1} \\ x_{3,t-1} \end{bmatrix} \\
&+ \underbrace{\begin{bmatrix} -r_1^2 & 0 & 0 \\ 0.7136 & -r_2^2 & 0 \\ 0 & 0.5 & -r_3^2 \end{bmatrix}}_{A_2} \begin{bmatrix} x_{1,t-2} \\ x_{2,t-2} \\ x_{3,t-2} \end{bmatrix} \\
&+ \underbrace{\begin{bmatrix} 0 & 0 & 0 \\ -0.356 & 0 & 0 \\ 0 & -0.3098 & 0 \end{bmatrix}}_{A_3} \begin{bmatrix} x_{1,t-3} \\ x_{2,t-3} \\ x_{3,t-3} \end{bmatrix} + \begin{bmatrix} w_{1,t} \\ w_{2,t} \\ w_{3,t} \end{bmatrix}
\end{aligned}$$

- sensor
- source



Multivariate autoregressive modelling (MVAR)

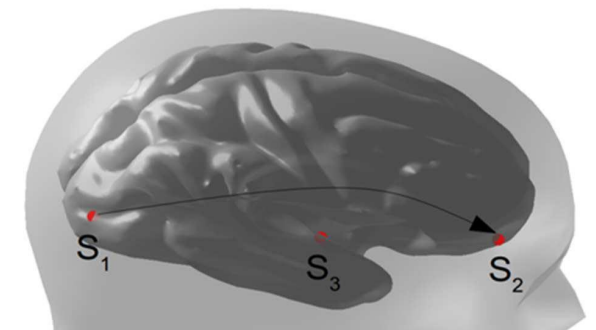
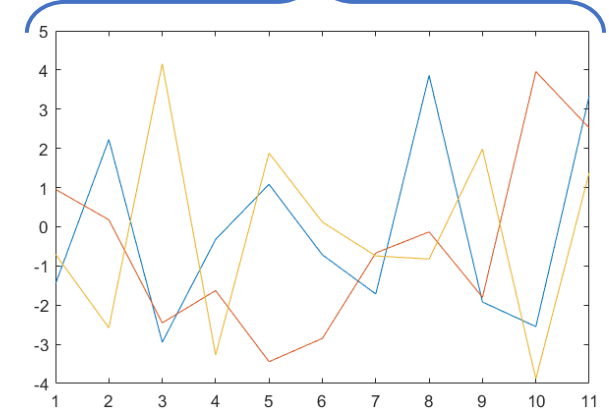


$$\begin{matrix}
 -0.3 & -1.6 & -3.3 \\
 1.1 & -3.4 & 1.9 \\
 -0.7 & -2.8 & 0.1 \\
 -1.7 & -0.7 & -0.7 \\
 \boxed{3.9} & \boxed{-0.1} & \boxed{-0.8} \\
 -1.9 & -1.8 & 2.0 \\
 -2.5 & 4.0 & -3.9 \\
 \boxed{3.3} & \boxed{2.5} & \boxed{1.4}
 \end{matrix}
 = \begin{matrix}
 -2.9 & -2.5 & 4.2 \\
 -0.3 & -1.6 & -3.3 \\
 1.1 & -3.4 & 1.9 \\
 -0.7 & -2.8 & 0.1 \\
 -1.7 & -0.7 & -0.7 \\
 \boxed{3.9} & \boxed{-0.1} & \boxed{-0.8} \\
 3.9 & -0.1 & -0.8 \\
 -1.9 & -1.8 & 2.0 \\
 \boxed{-2.5} & \boxed{4.0} & \boxed{-3.9}
 \end{matrix} * \mathbf{A}_1 + \begin{matrix}
 2.2 & 0.2 & -2.6 \\
 -2.9 & -2.5 & 4.2 \\
 -0.3 & -1.6 & -3.3 \\
 1.1 & -3.4 & 1.9 \\
 -0.7 & -2.8 & 0.1 \\
 -1.7 & -0.7 & -0.7 \\
 3.9 & -0.1 & -0.8 \\
 -1.9 & -1.8 & 2.0
 \end{matrix} * \mathbf{A}_2 + \begin{matrix}
 -1.5 & \textcolor{red}{1.0} & \textcolor{orange}{-0.7} \\
 2.2 & \textcolor{red}{0.2} & \textcolor{orange}{-2.6} \\
 -2.9 & \textcolor{red}{-2.5} & \textcolor{orange}{4.2} \\
 -0.3 & \textcolor{red}{-1.6} & \textcolor{orange}{-3.3} \\
 1.1 & \textcolor{red}{-3.4} & \textcolor{orange}{1.9} \\
 -0.7 & \textcolor{red}{-2.8} & \textcolor{orange}{0.1} \\
 -1.7 & \textcolor{red}{-0.7} & \textcolor{orange}{-0.7} \\
 \boxed{3.9} & \textcolor{red}{-0.1} & \textcolor{orange}{-0.8}
 \end{matrix} * \mathbf{A}_3 + \mathbf{E}$$

\mathbf{Y}_t \mathbf{Y}_{t-1} \mathbf{Y}_{t-2} \mathbf{Y}_{t-3}

By setting $\mathbf{Y} = \mathbf{Y}_t$, $\mathbf{X} = [\mathbf{Y}_{t-1}, \mathbf{Y}_{t-2}, \mathbf{Y}_{t-3}]$, and $\mathbf{B} = [\mathbf{A}_1; \mathbf{A}_2; \mathbf{A}_3]$

$$\mathbf{Y} = \mathbf{XB} + \mathbf{E} \quad \xrightarrow{\hspace{1cm}} \quad \mathbf{B} = (\mathbf{X}^T \mathbf{X})^{-1} \mathbf{X}^T \mathbf{Y}$$



Linear models: $\mathbf{y} = \mathbf{X}\boldsymbol{\beta} + \boldsymbol{\varepsilon}; \boldsymbol{\varepsilon} \sim N(\mathbf{0}, \sigma^2 \mathbf{I})$

TABLE 3.2. Linear model fit to the prostate cancer data.

The Z score is the coefficient divided by its standard error (3.12). Roughly a Z score larger than two in absolute value is significantly nonzero at the $p = 0.05$ level.

Term	Coefficient	Std. Error	Z Score
Intercept	2.46	0.09	27.60
lcavol	0.68	0.13	5.37
lweight	0.26	0.10	2.75
age	-0.14	0.10	-1.40
lbph	0.21	0.10	2.06
svi	0.31	0.12	2.47
lcp	-0.29	0.15	-1.87
gleason	-0.02	0.15	-0.15
pgg45	0.27	0.15	1.74

lpsa: log of prostate-specific antigen

lcavol: log of cancer volume

lweight: log of prostate weight

lbph: log of (amount) benign prostatic hyperplasia

svi: seminal vesicle invasion

lcp: log of capsular penetration

pgg45: percent of Gleason scores 4 or 5

$$\begin{aligned} lpsa = & \beta_0 + \beta_1 lcavol + \beta_2 lweight + \beta_3 age + \beta_4 lbph \\ & + \beta_5 svi + \beta_6 lcp + \beta_7 gleason + \beta_8 pgg45 \end{aligned}$$

By removing non-significant variables: *age*, *lcp*, *gleason* and *pgg45*:

$$lpsa = \gamma_0 + \gamma_1 lcavol + \gamma_2 lweight + \gamma_4 lbph + \gamma_5 svi$$

We get

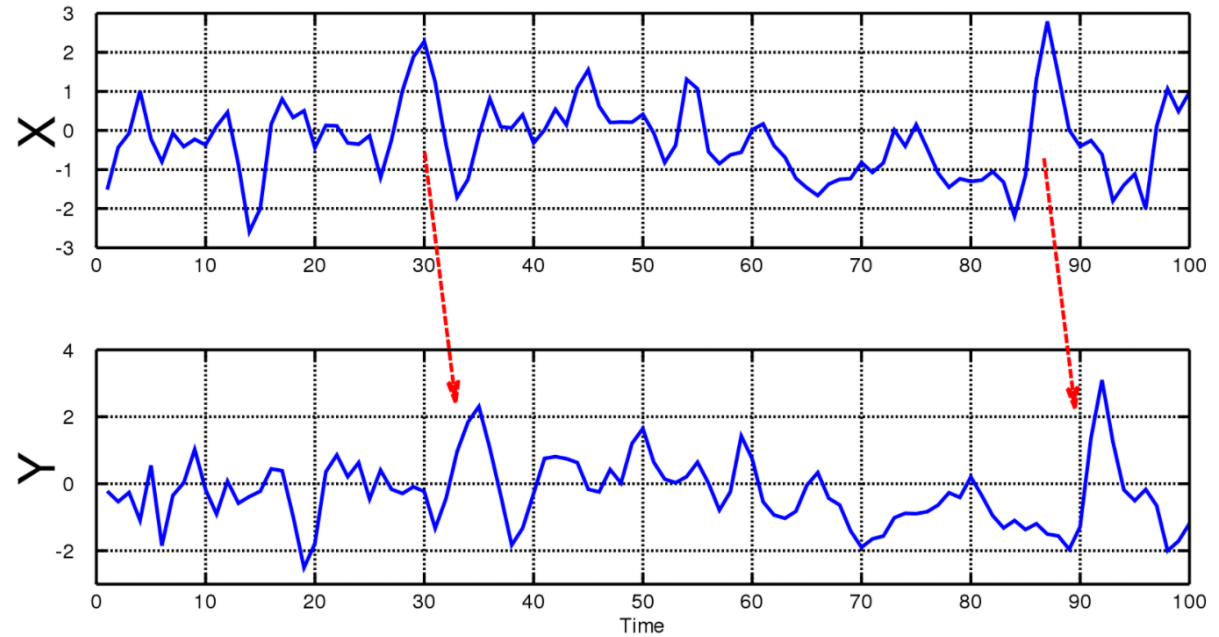
$$F = \frac{(32.81 - 29.43)/(9 - 5)}{29.43/(67 - 9)} = 1.67$$

which has a p-value of 0.17 ($\Pr(F_{4,58} > 1.67) = 0.17$)

Granger causality

According to Granger causality, if a signal **X** “Granger-causes” **Y**, then past values of **X** should contain information that helps predict **Y** above and beyond the information contained in past values of **Y** alone.

http://www.scholarpedia.org/article/Granger_causality



https://en.wikipedia.org/wiki/Granger_causality

Granger causality test:

Reduced model: $Y_t = \alpha_0 + \alpha_1 Y_{t-1} + \alpha_2 Y_{t-2} + \dots + \alpha_p Y_{t-p} + \varepsilon_t$

Full model:

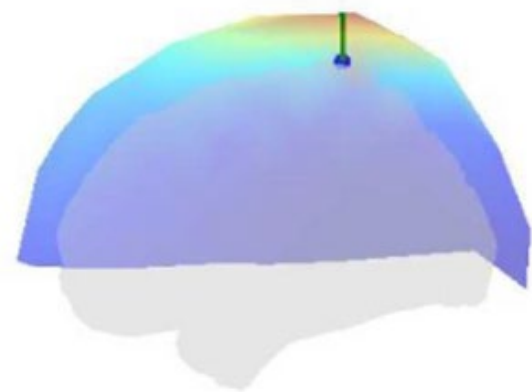
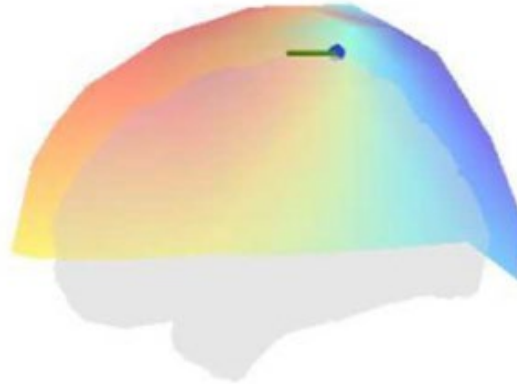
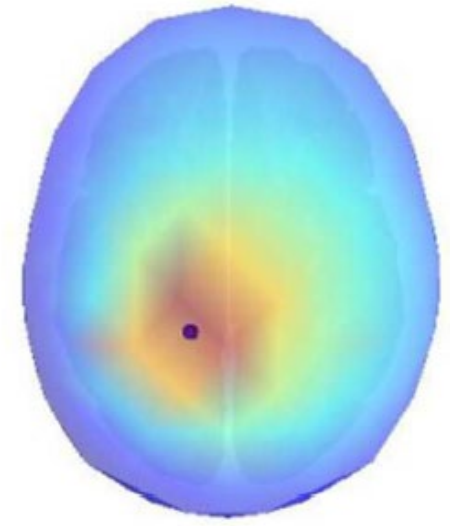
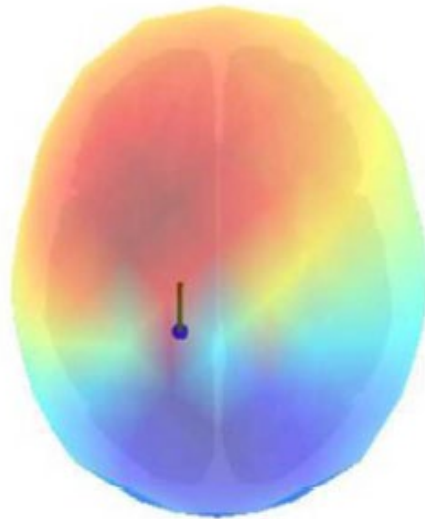
$$Y_t = \beta_0 + \beta_1 Y_{t-1} + \beta_2 Y_{t-2} + \dots + \beta_p Y_{t-p} + \gamma_1 X_{t-1} + \gamma_2 X_{t-2} + \dots + \gamma_p X_{t-p} + \sigma_t$$

Model order parameter (p) is estimated for the full model using criteria such as AIC, BIC, GCV.

State-space (SS) models (linear):

$$S(t) = \sum_{d=1}^p \mathbf{A}(d)S(t-d) + U(t)$$

$$Y(t) = \mathbf{L}S(t) + G(t)$$



Van de Steen, F., Faes, L., Karahan, E., Songsiri, J., Valdes-Sosa, P.A. and Marinazzo, D., 2019. Critical comments on EEG sensor space dynamical connectivity analysis. *Brain topography*, 32(4), pp.643-654

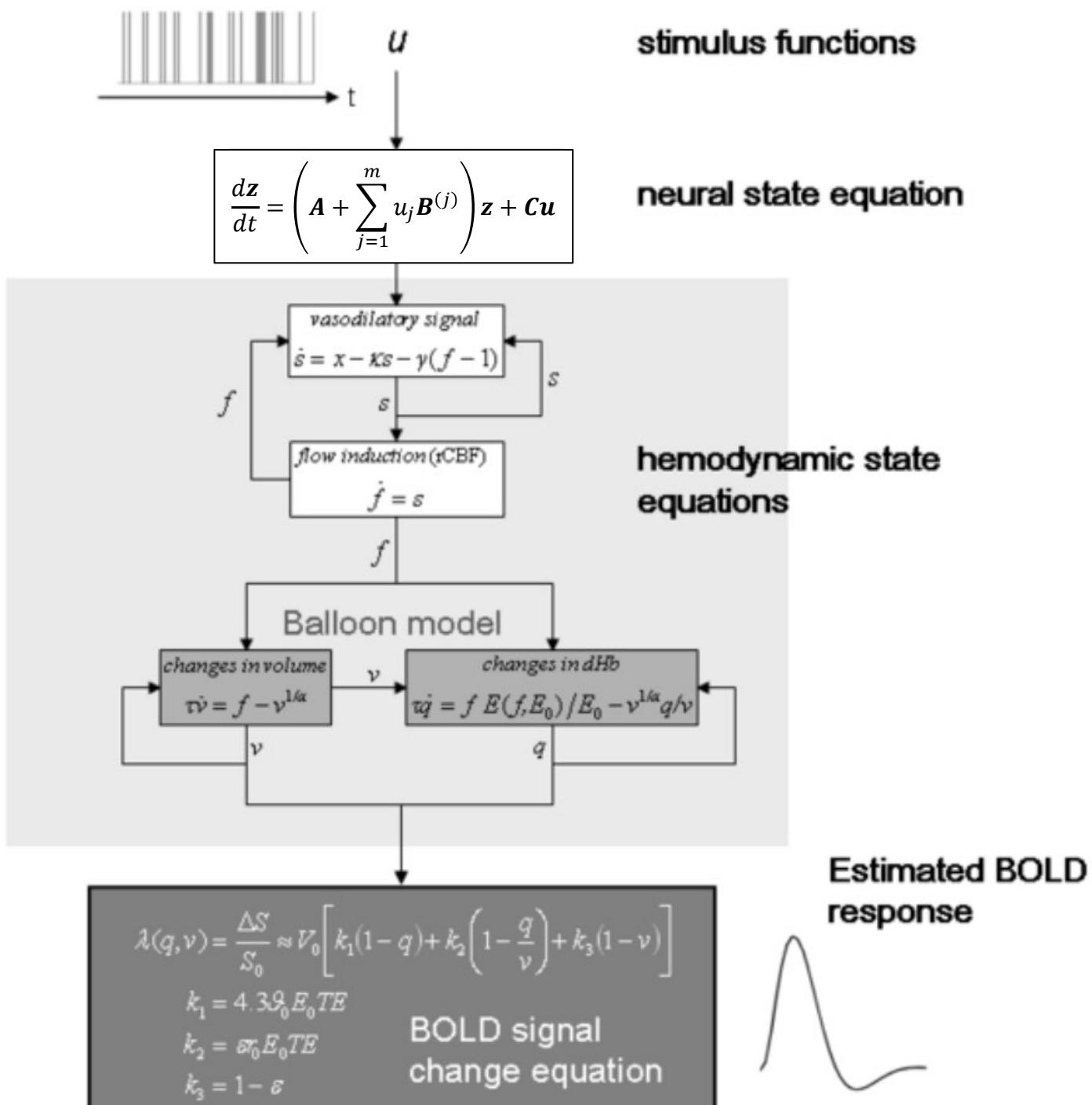
Hemodynamic model

Friston, K.J., Harrison, L. and Penny, W., 2003. Dynamic causal modelling. *Neuroimage*, 19(4), pp.1273-1302.

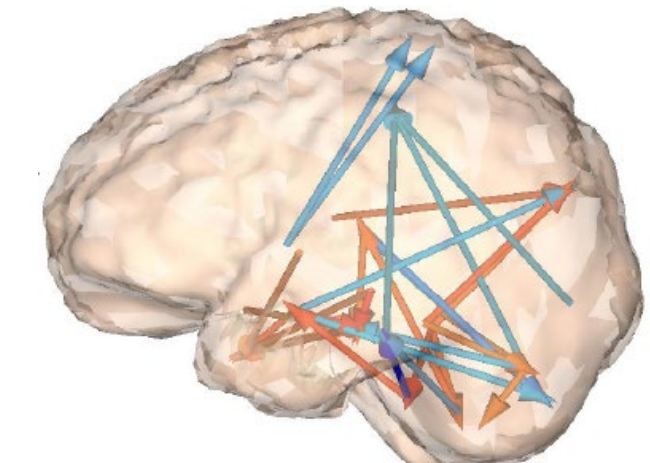
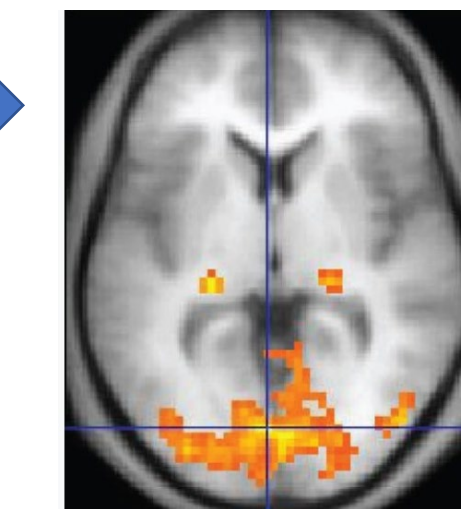
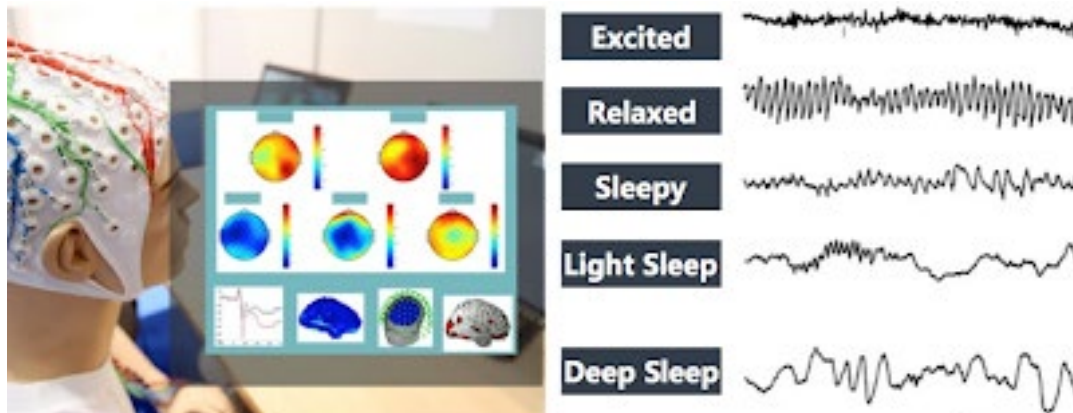
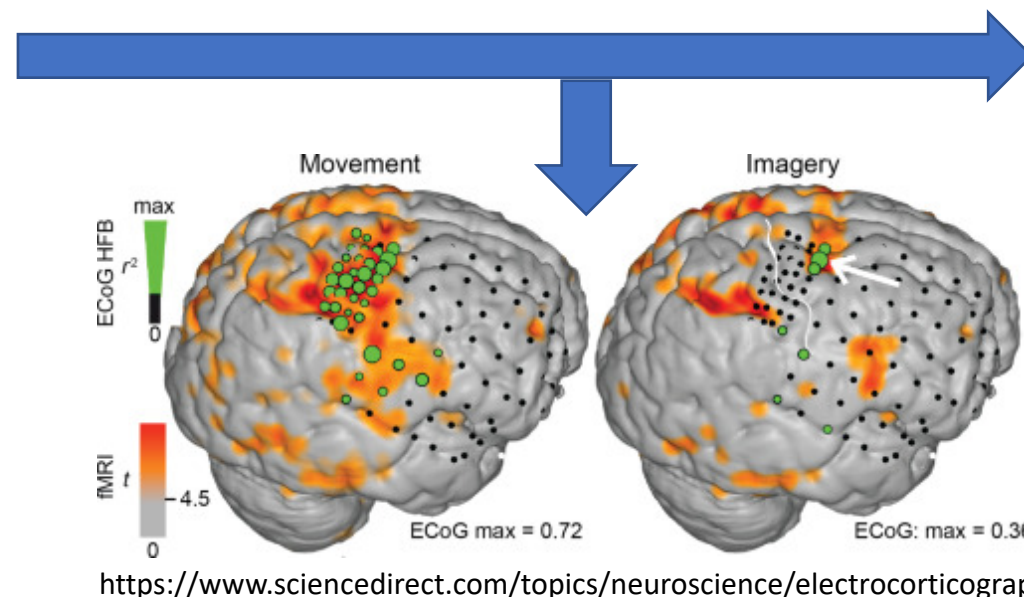
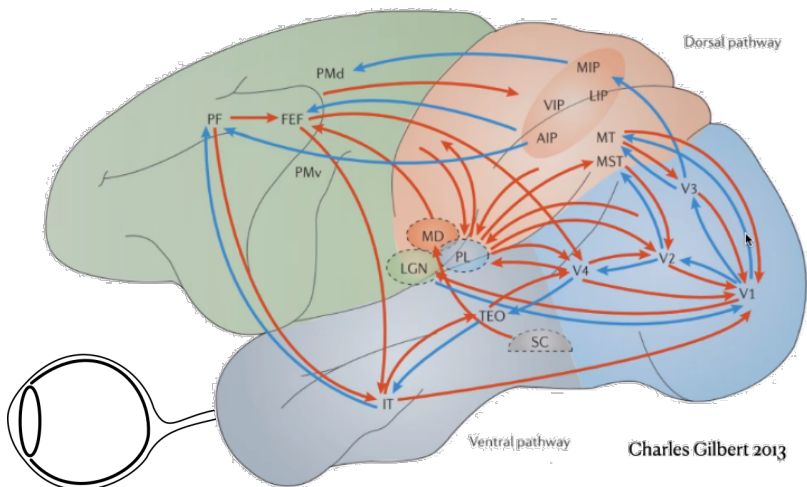
See also:

http://www.scholarpedia.org/article/Dynamic_causal_modeling

This schematic shows the architecture of the hemodynamic model for a single region. Neuronal activity induces a vasodilatory and activity-dependent signal s that increases the flow f . Flow causes changes in volume and deoxyhemoglobin (v and q). These two hemodynamic states enter the output nonlinearity Eq. (4) to produce the observed BOLD response y .



Connectivity Between Areas Involved in Visual Processing



Brain anatomical
connectivity

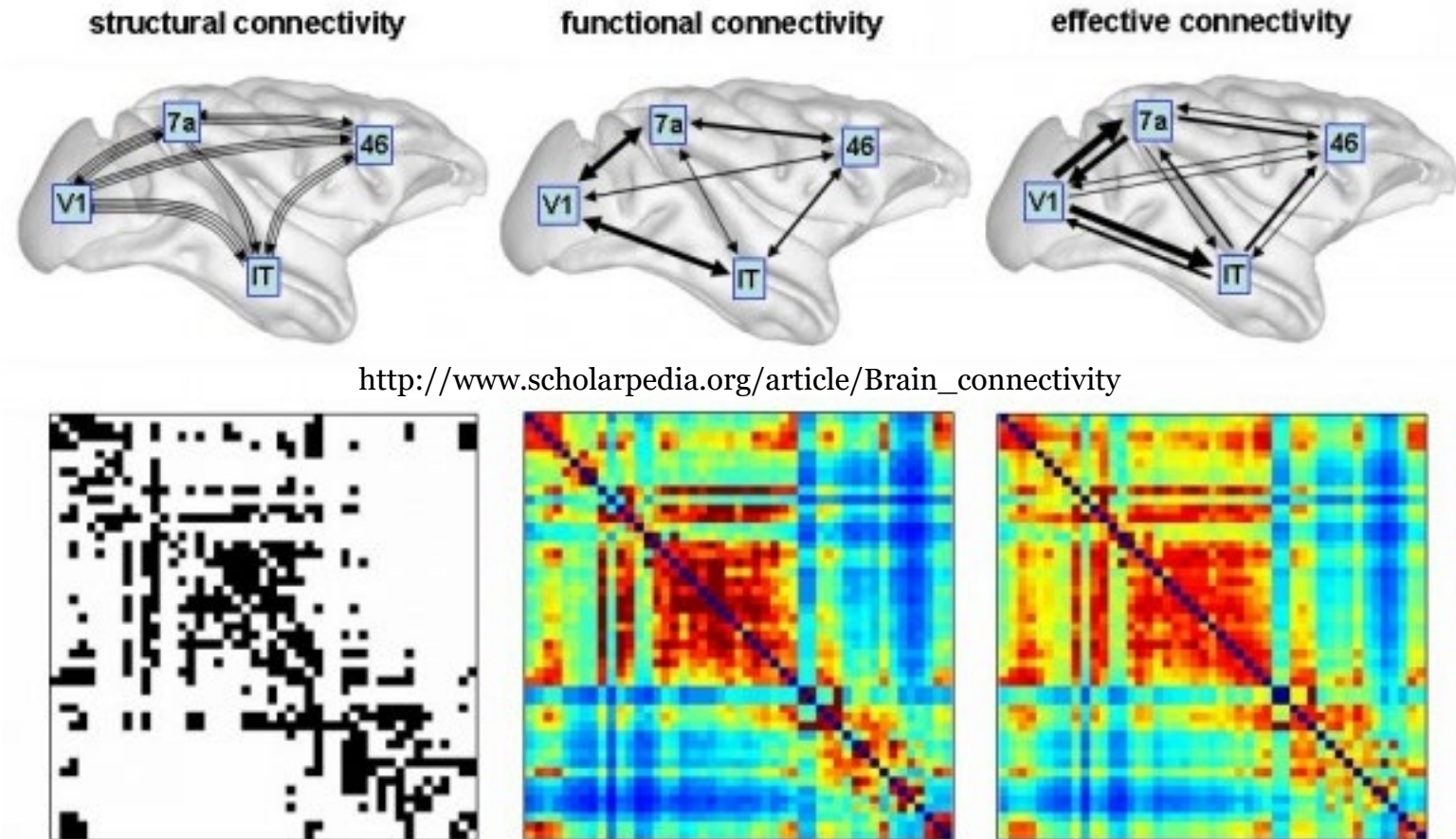
Concepts:

structural connectivity: sparse and directed graph. **Weighted:** weights represent connection densities. **Binary:** entries indicate the presence or absence of a connection.

functional connectivity: full symmetric matrix. Each entry encodes statistical dependency between two nodes (neurons, recording sites, voxels). It may be thresholded to yield sparse graphs (undirected), with the setting of the threshold controlling the degree of sparsity.

effective connectivity: full asymmetric matrix. Applying a threshold to such matrices yields sparse directed graphs.

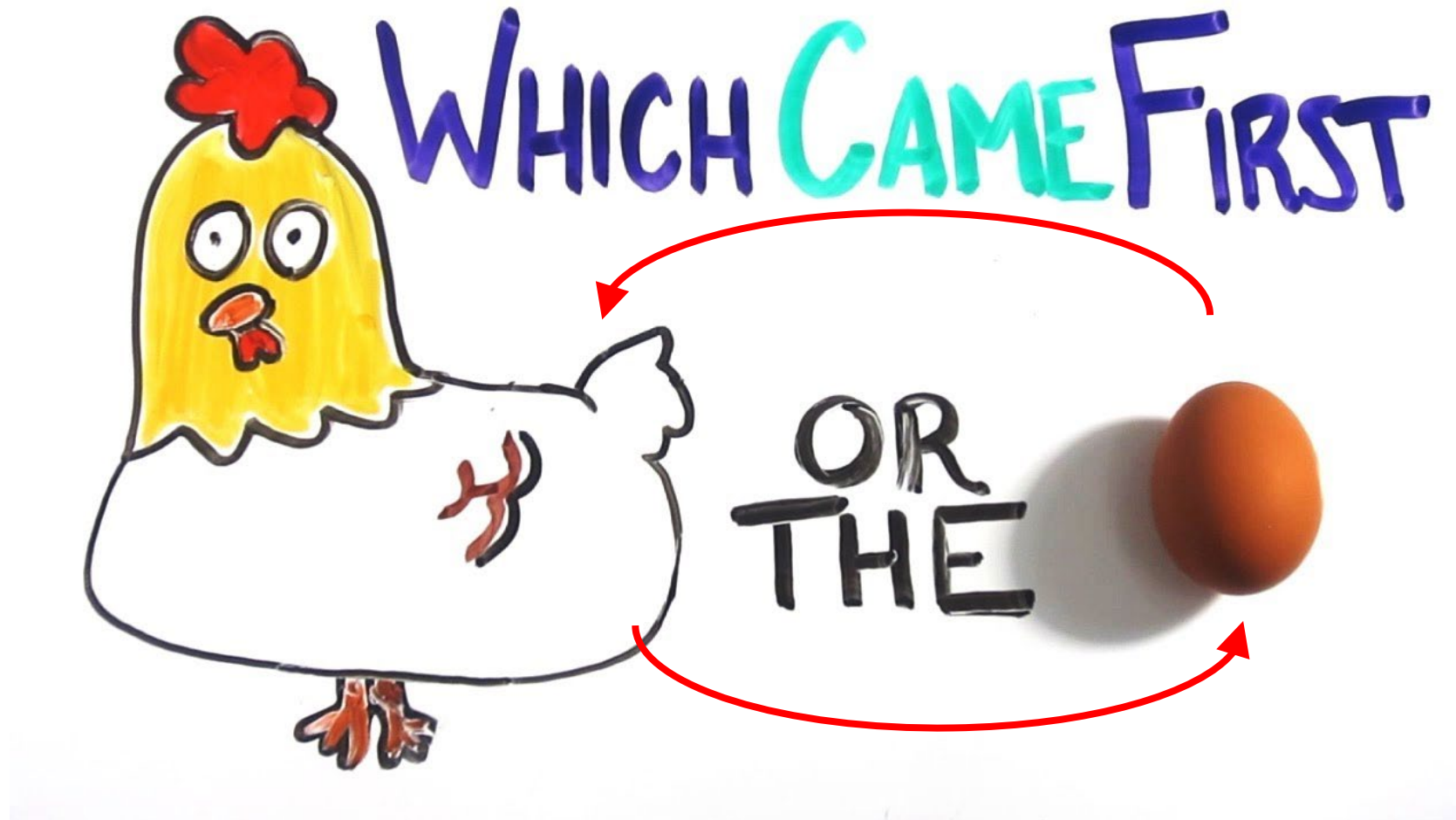
http://www.scholarpedia.org/article/Brain_connectivity



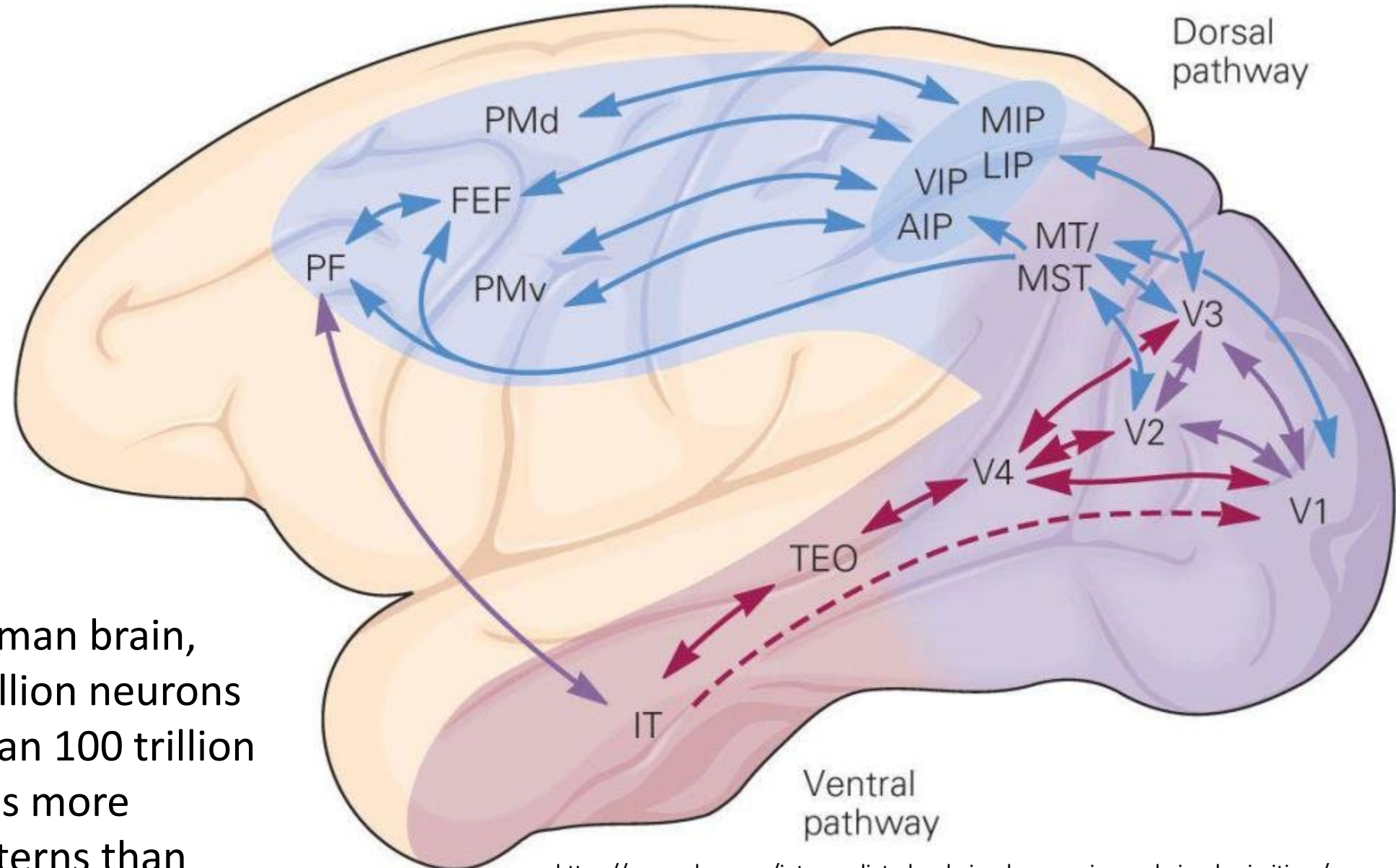
Directed functional connectivity, for example, Granger causality (GC) (Granger, 1969), assesses the recurrent functional integration, among different brain areas. This approach is exploratory and rests on the notion of predictability and statistical dependencies to establish causal relationships. On the contrary, effective connectivity, as measured with dynamic causal modeling (DCM) (Friston et al., 2003), considers the influence of one neural system over the other.

Bajaj, S, Adhikari, BM, Friston, KJ and Dhamala, M, 2016. Bridging the gap: dynamic causal modeling and granger causality analysis of resting state functional magnetic resonance imaging. *Brain connectivity*, 6(8), pp.652-661.

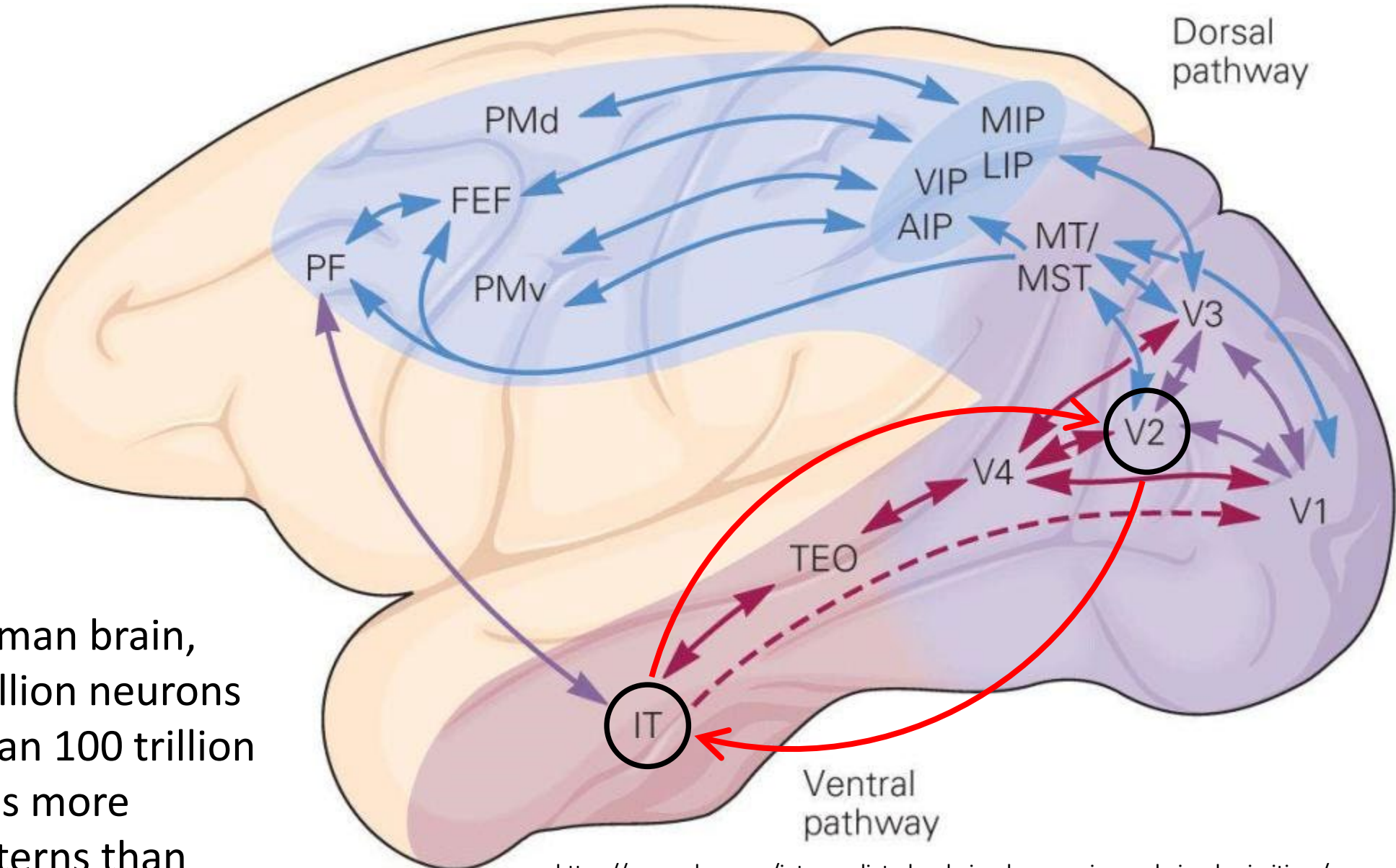
Why is it important to understand brain (anatomical) connectivity?



<https://www.krcu.org/post/chicken-or-egg#stream/0>

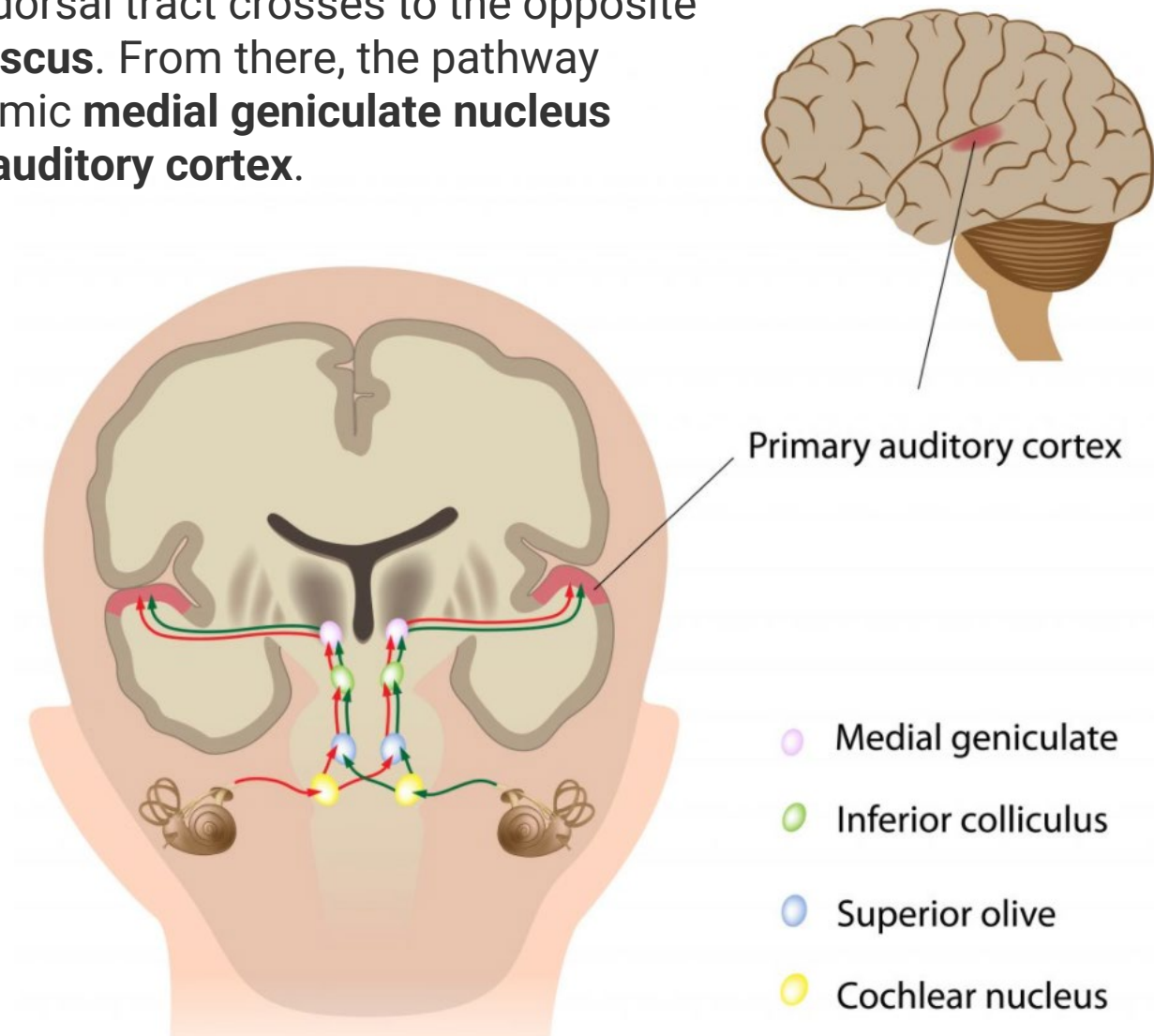
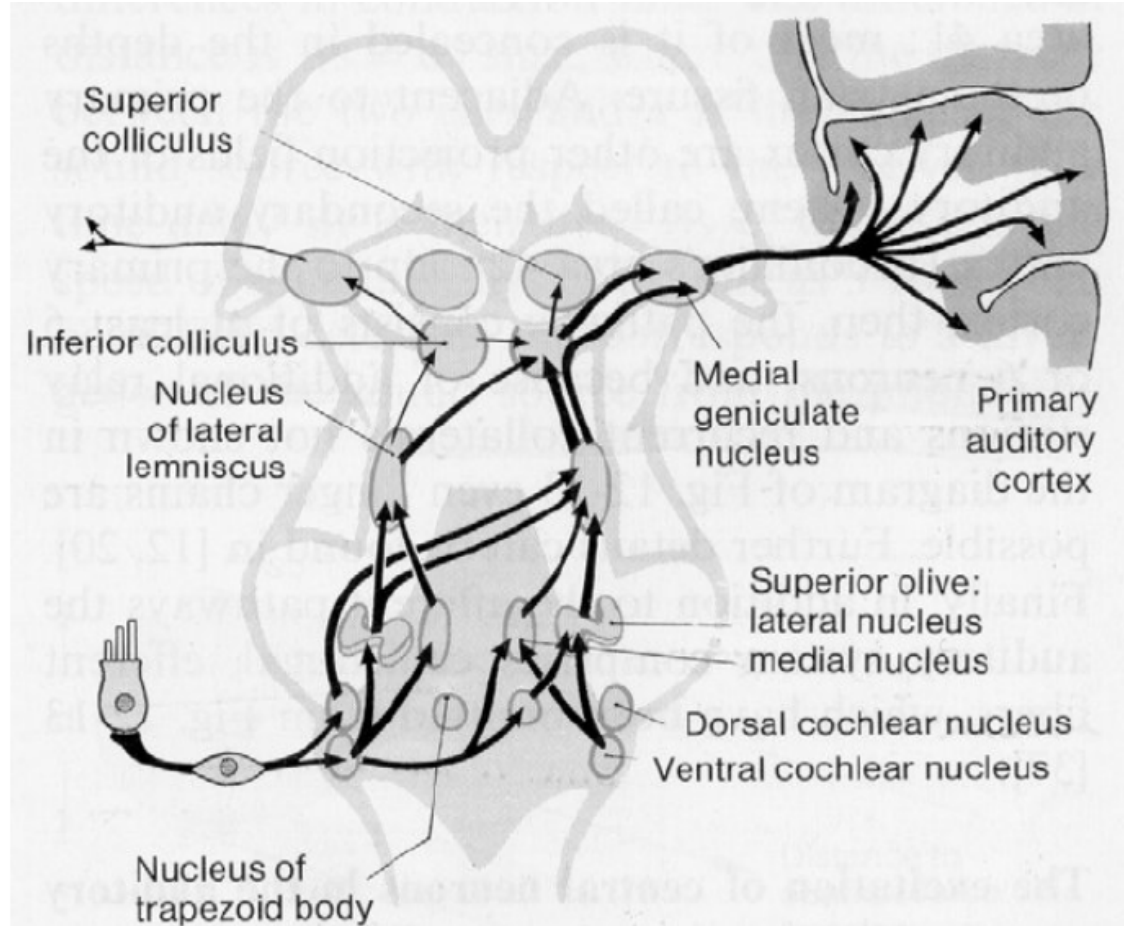


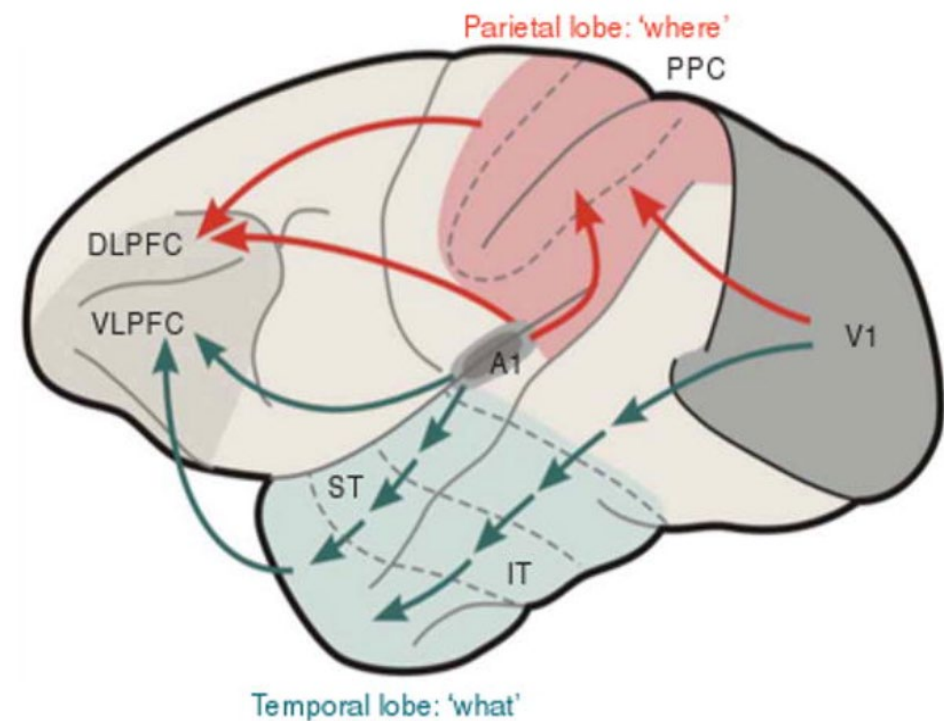
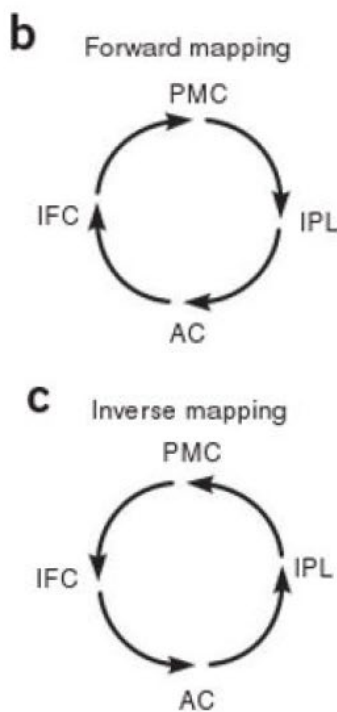
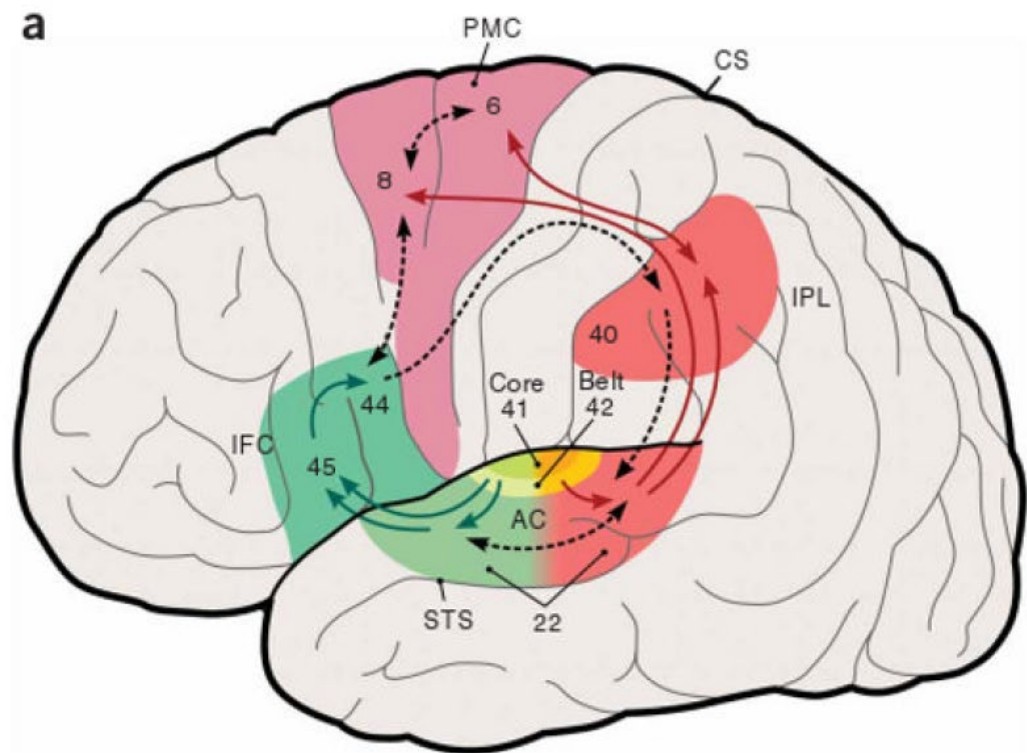
Fact: The human brain, with \approx 100 billion neurons and more than 100 trillion synapses, has more complex patterns than ever hypothesized.



Fact: The human brain, with \approx 100 billion neurons and more than 100 trillion synapses, has more complex patterns than ever hypothesized.

Diagram of the subcortical auditory pathway. The auditory nerve bifurcates after leaving the **cochlea**, sending one branch into the **ventral cochlear nucleus** and the other into the adjacent **dorsal cochlear nucleus**. From the ventral cochlear nucleus, a ventral tract runs to the ipsi- and contralateral **olivary complexes** and ascends to the nucleus of the **lateral lemniscus**. From the dorsal cochlear nucleus, a dorsal tract crosses to the opposite side and ascends further to the nucleus of the **lateral lemniscus**. From there, the pathway proceeds through the midbrain **inferior colliculus** and thalamic **medial geniculate nucleus** (*music goes to medial and light goes to lateral*) to the **primary auditory cortex**.



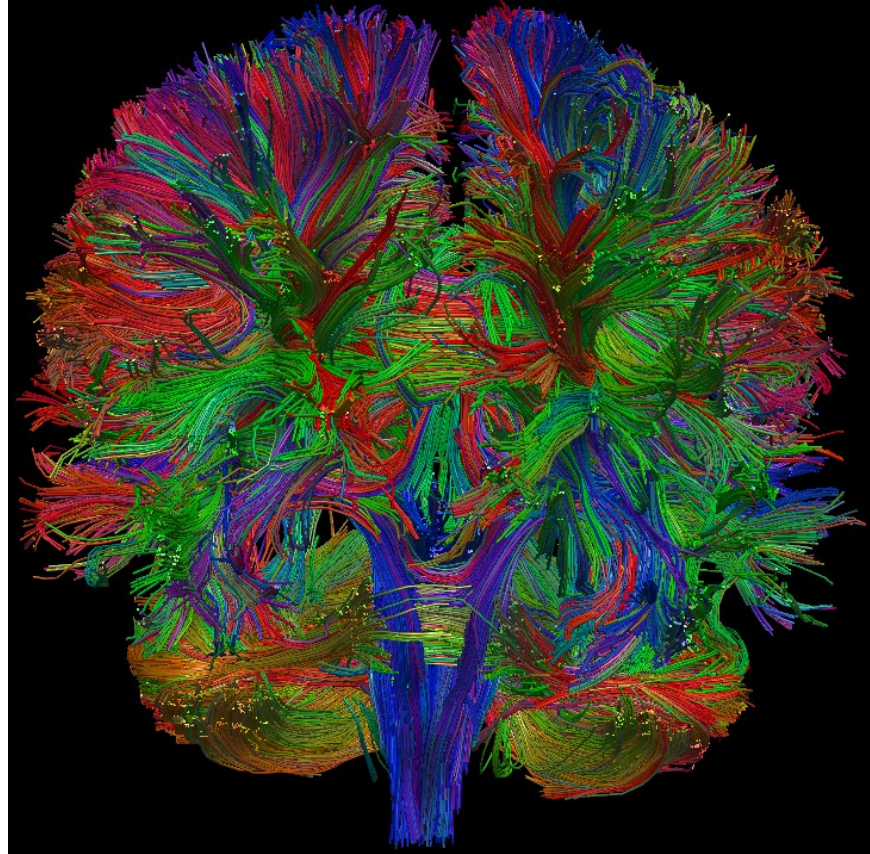


(a) Antero-ventral (green) and postero-dorsal (red) streams originating from the auditory belt. **(b)** In one direction, forward mapping, object information, such as speech, is decoded in the anteroventral stream all the way to category-invariant inferior frontal cortex (area 45), and is transformed into motor-articulatory representations (area 44 and ventral PMC), whose activation is transmitted to the IPL (and posterior superior temporal cortex) as an efference copy. **(c)** In reverse direction, the model performs an inverse mapping, whereby attention- or intention-related changes in the IPL influence the selection of context-dependent action programs in PFC and PMC.

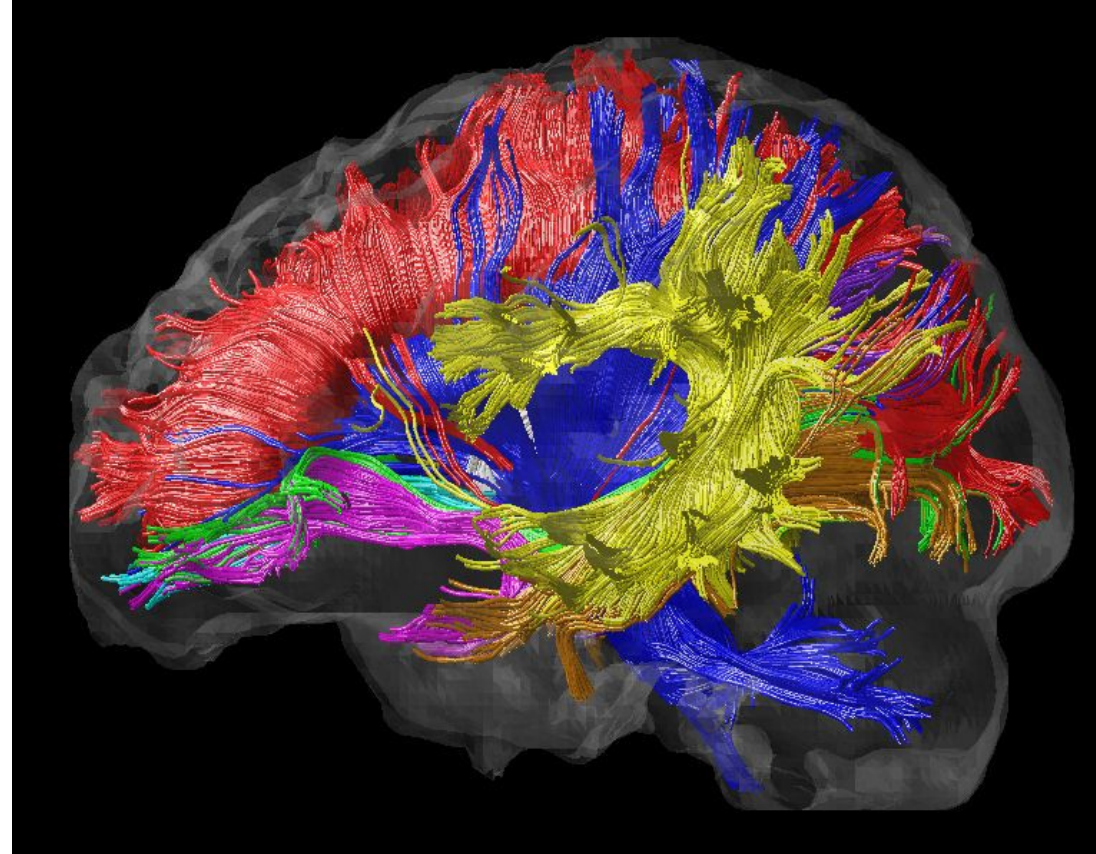
Dual processing scheme for 'what' and 'where', proposed for nonhuman primates on anatomical and physiological grounds.

Rauschecker, J.P. and Scott, S.K., 2009. Maps and streams in the auditory cortex: nonhuman primates illuminate human speech processing. *Nature neuroscience*, 12(6), pp.718-724

Diffusion tensor imaging (DTI)



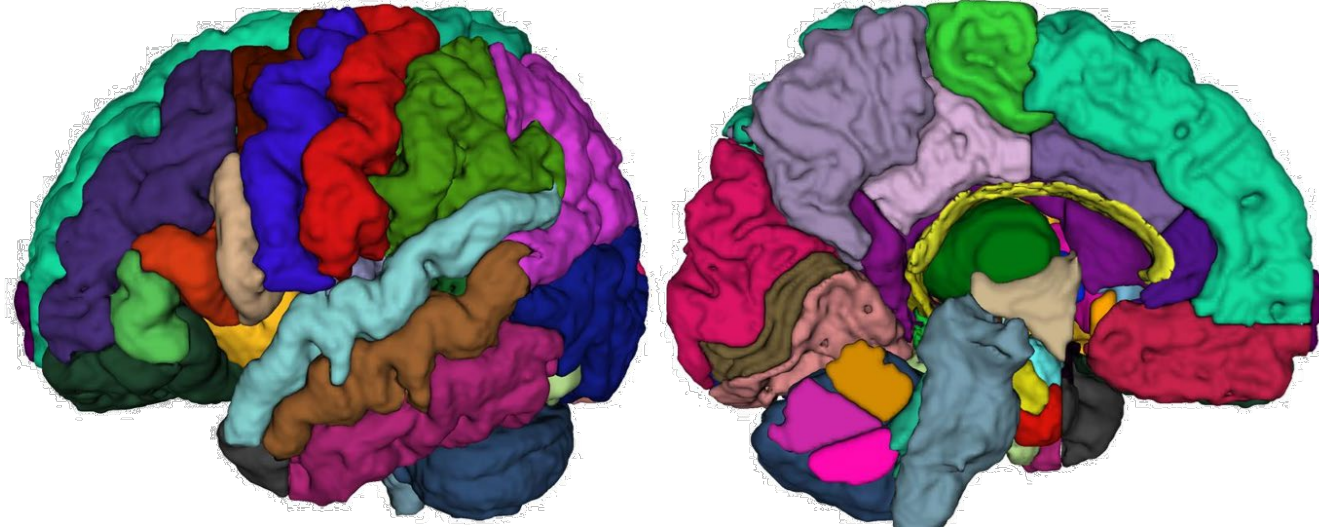
https://www.reddit.com/r/ScienceImages/comments/3exjme/diffusion_tensor_imaging_dti_of_human_brain/



<https://www.pinterest.com/pin/148829962659610552/>

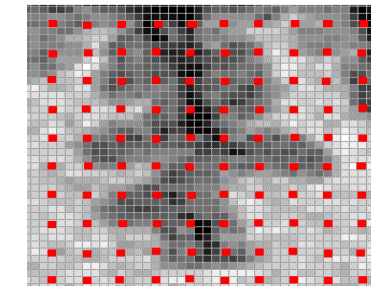
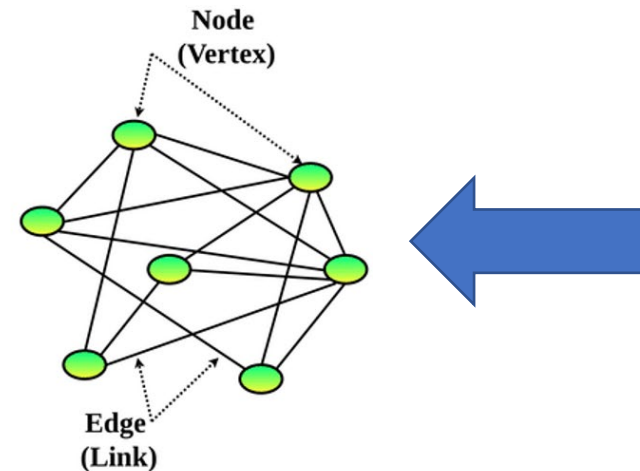
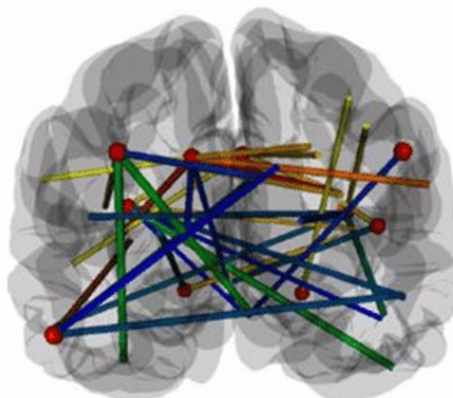
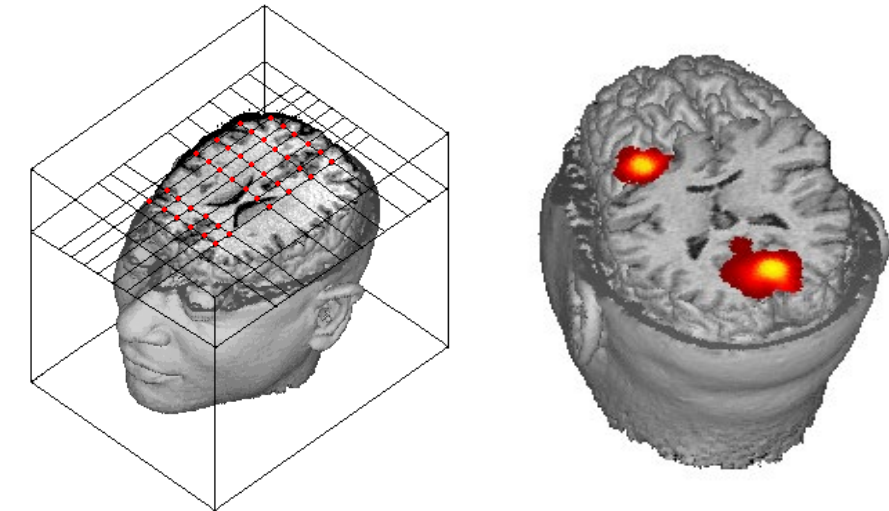
Resting-state functional
connectivity

Atlas – Regions/Voxels – Graphical representation



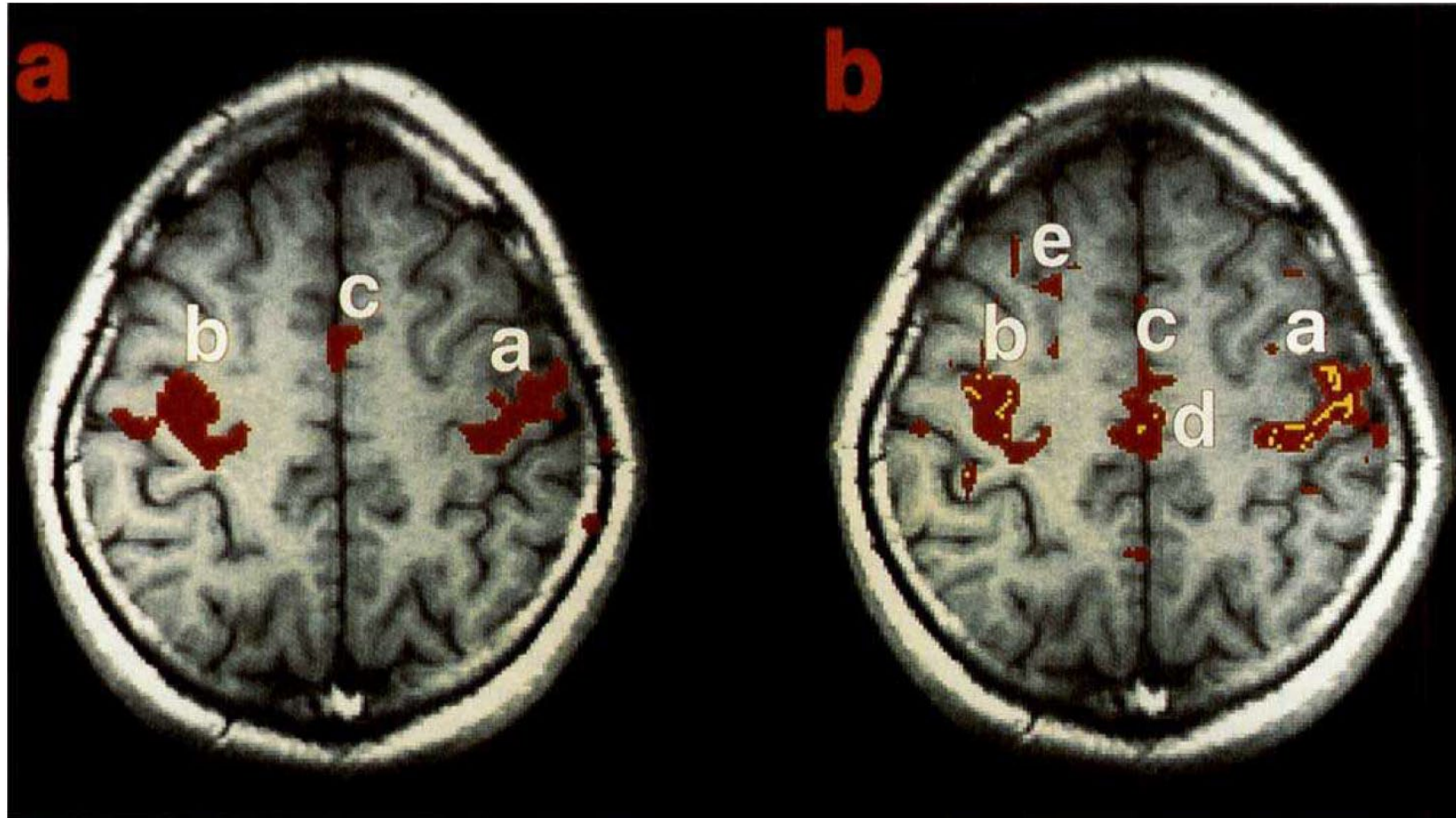
Tahmassebi, Amirhessam, et al. "Determining disease evolution driver nodes in dementia networks." *Medical Imaging 2018: Biomedical Applications in Molecular, Structural, and Functional Imaging*. Vol. 10578. International Society for Optics and Photonics, 2018.

Alexander, Bonnie, et al. "Desikan-Killiany-Tourville atlas compatible Version of M-CRIB neonatal parcellated whole brain atlas: the M-CRIB 2.0." *Frontiers in neuroscience* 13 (2019): 34

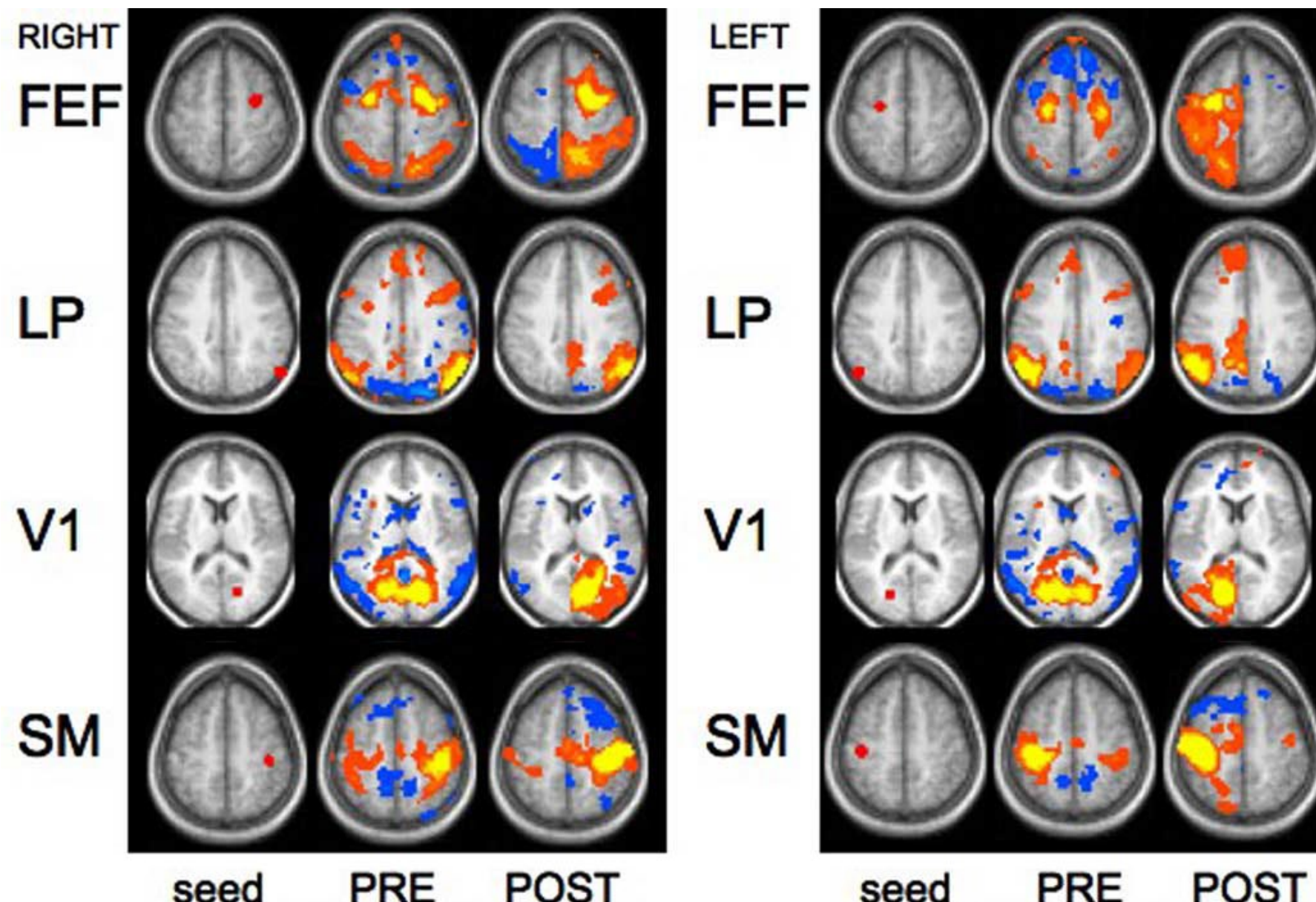


Voxelwise
analyses

Resting state functional MRI (rsfMRI)

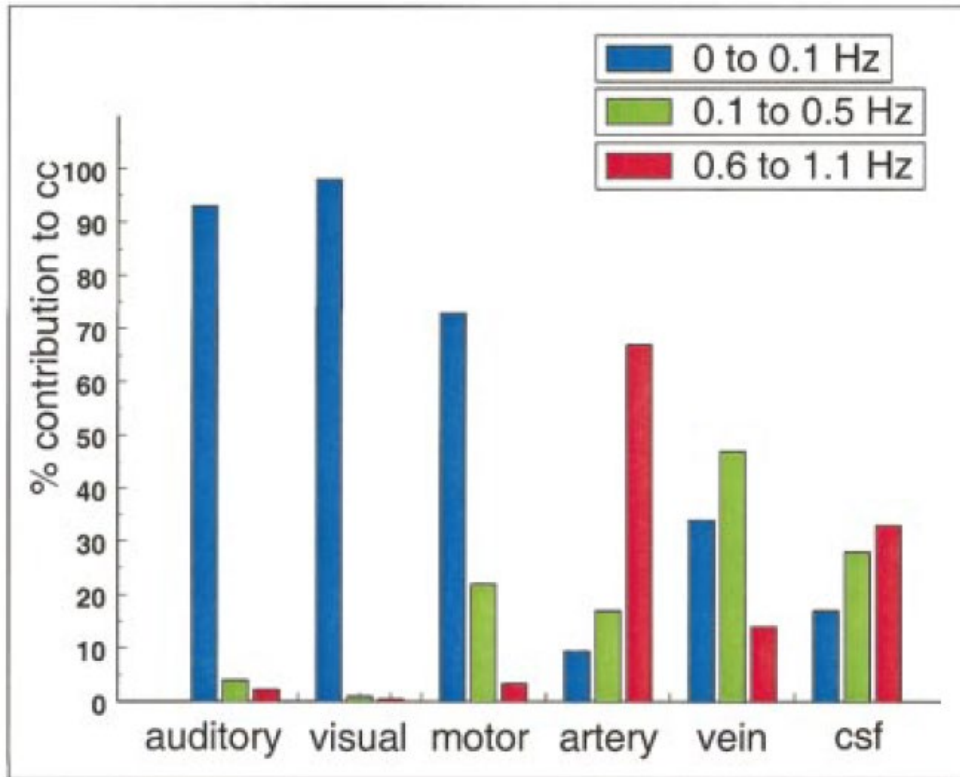


Biswal, Bharat, et al. "Functional connectivity in the motor cortex of resting human brain using echo-planar MRI." *Magnetic resonance in medicine* 34.4 (1995): 537-541.



Johnston, James M., et al. "Loss of resting interhemispheric functional connectivity after complete section of the corpus callosum." *Journal of Neuroscience* 28.25 (2008): 6453-6458.

Can rsfMRI be confidently linked to brain activity?



Cordes, Dietmar, et al. "Frequencies contributing to functional connectivity in the cerebral cortex in "resting-state" data." American journal of neuroradiology 22.7 (2001): 1326-1333.

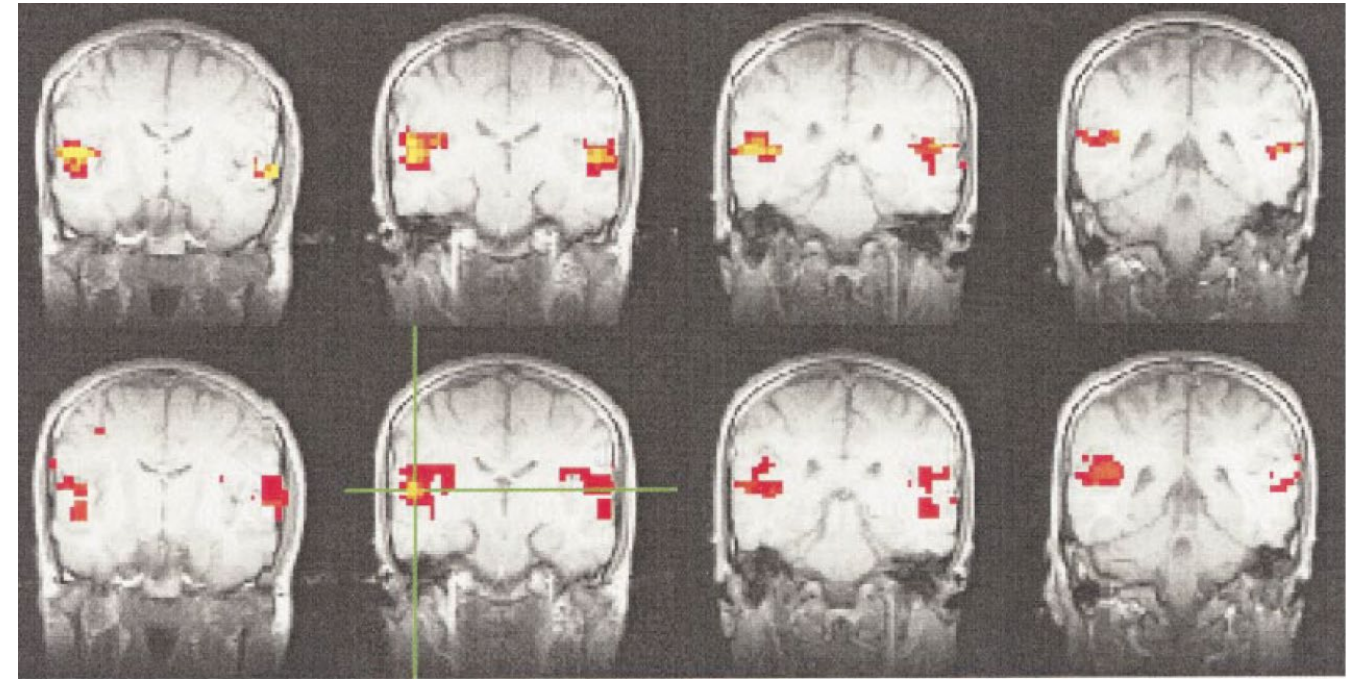


FIG 1: Typical examples of task-activation maps (top) and rsfMRI maps (bottom) for four contiguous slices (TR=500 ms). Auditory cortex activation and FC maps showed very similar spatial distributions across different slices .

FIG 11. Contribution of low frequencies (0 to 0.1 Hz), respiratory frequencies (0.1 to 0.5 Hz), and cardiac frequencies to the cross-correlation coefficient in different ROIs in the same subject. Low-frequency components clearly dominate, contributing to functional connectivity in auditory, visual, and motor cortices. For blood vessels and cerebrospinal fluid, low-frequency components are present, but cardiac and respiratory noise sources are the main contributors.

Can rsfMRI be confidently linked to brain activity?

<https://www.youtube.com/watch?v=5yDN2q7gUaM>
https://www.youtube.com/watch?v=_867wiM_kLY
<https://www.youtube.com/watch?v=Nl5V2WsDyF0>

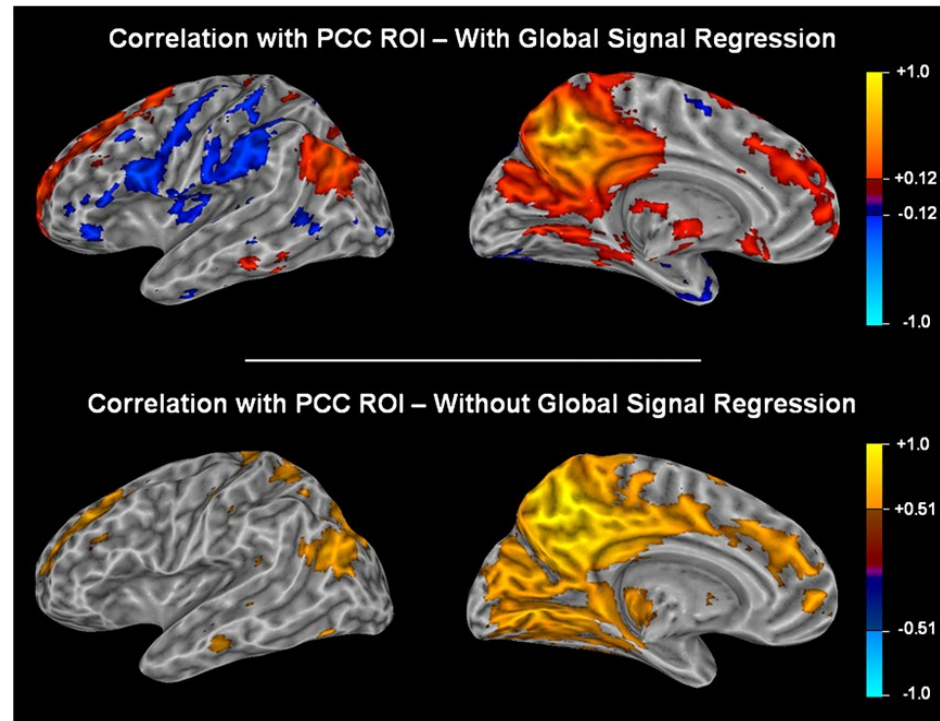


Fig. 6. Correlations to a seed region in the PCC averaged across all subjects using a Fisher transform are shown with and without correction for the global signal

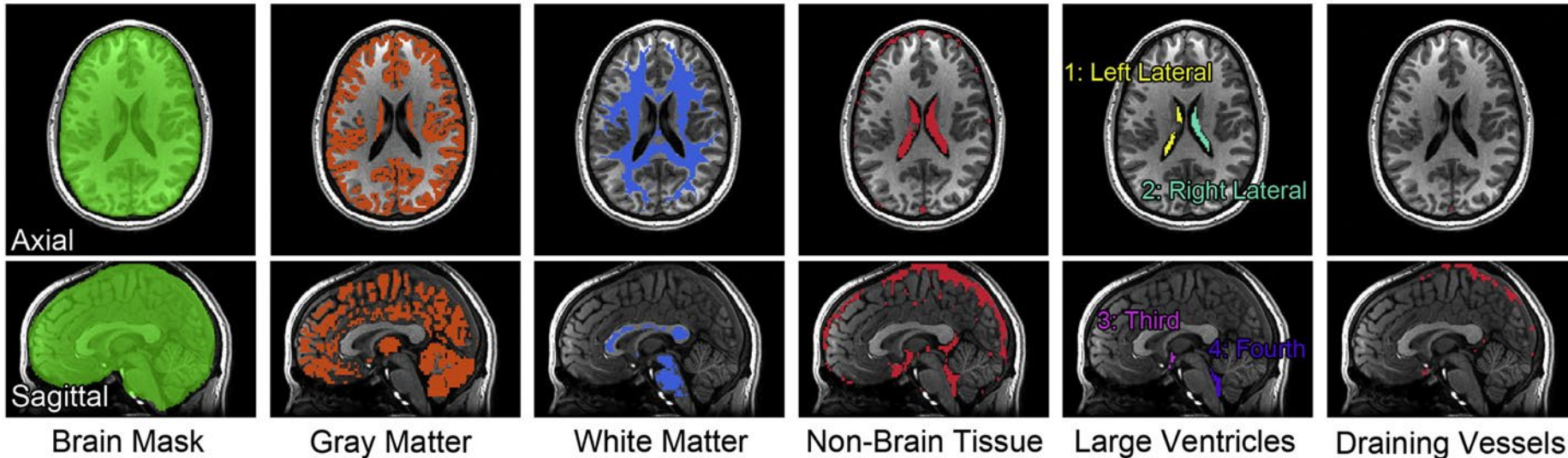


Fig. 1. Anatomically segmented masks for one subject. The masks (colored voxels) were defined on the T1 images, and then resampled to EPI's grid space. See the text for the details

rsfMRI (seed-based and ICA) and PET analysis to study brain networks

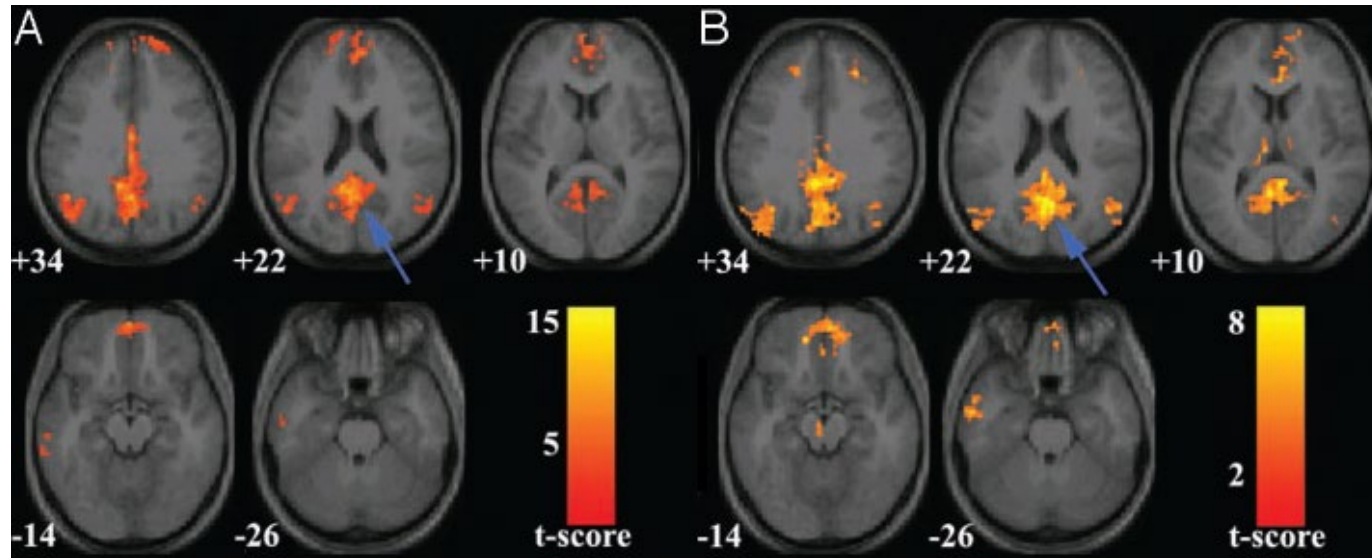


Fig. 1. Validation of the ICA approach (Stanford University data). Axial images showing the default-mode network as detected with ROI-based (A) and ICA-based (B) approaches in a group of healthy young adults scanned on a 3-T magnet at Stanford University. The blue arrows indicate the posterior cingulate cortex..

Greicius, Michael D., et al. "Default-mode network activity distinguishes Alzheimer's disease from healthy aging: evidence from functional MRI." PNAS 101.13 (2004): 4637-4642

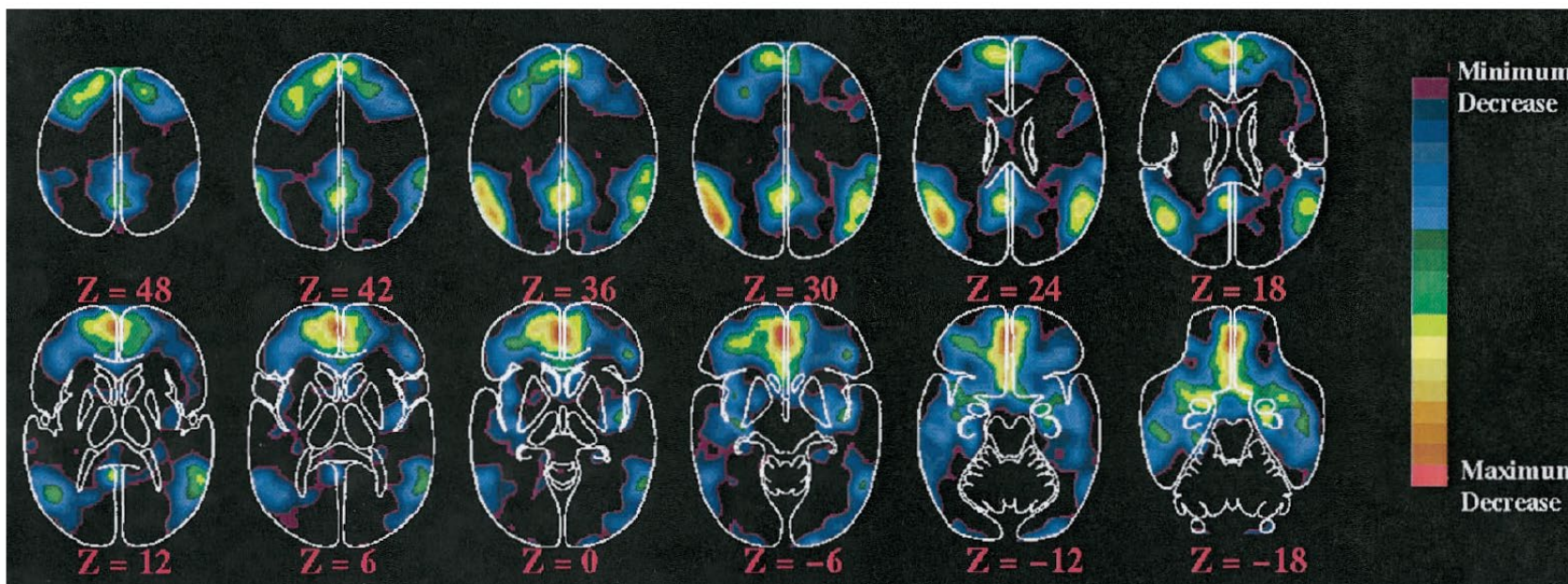
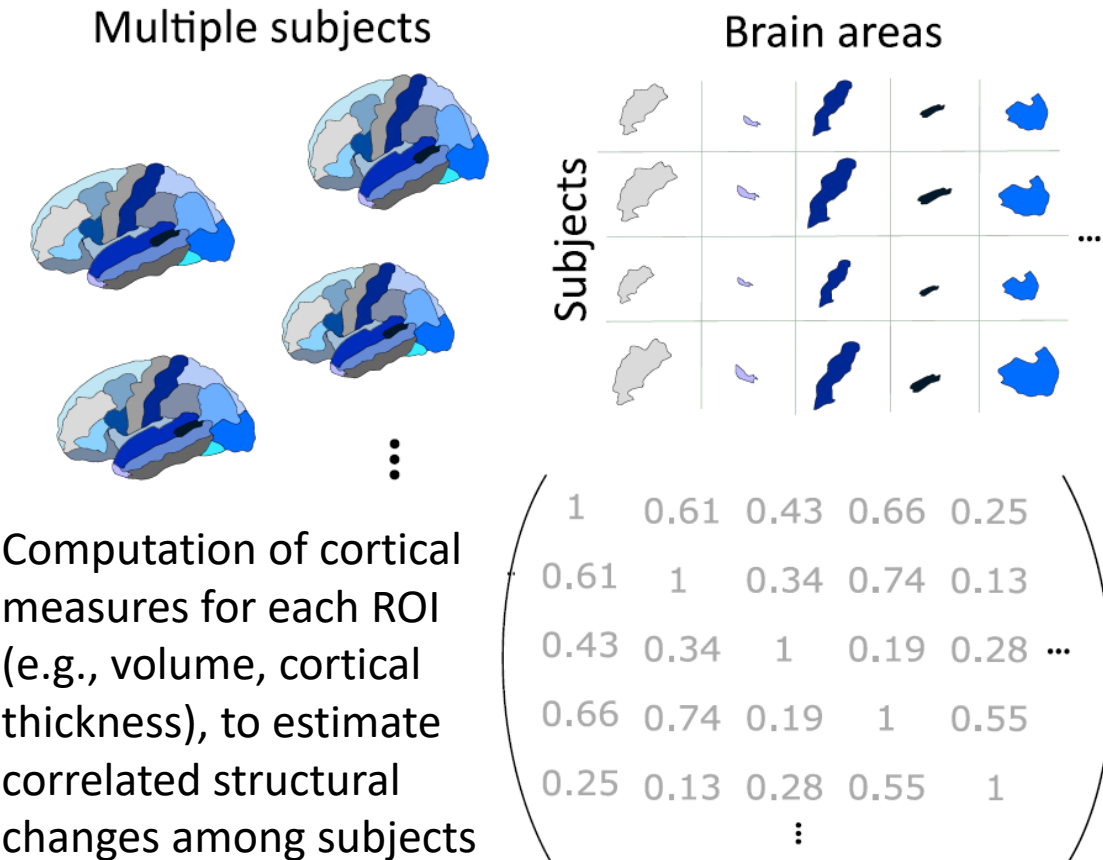


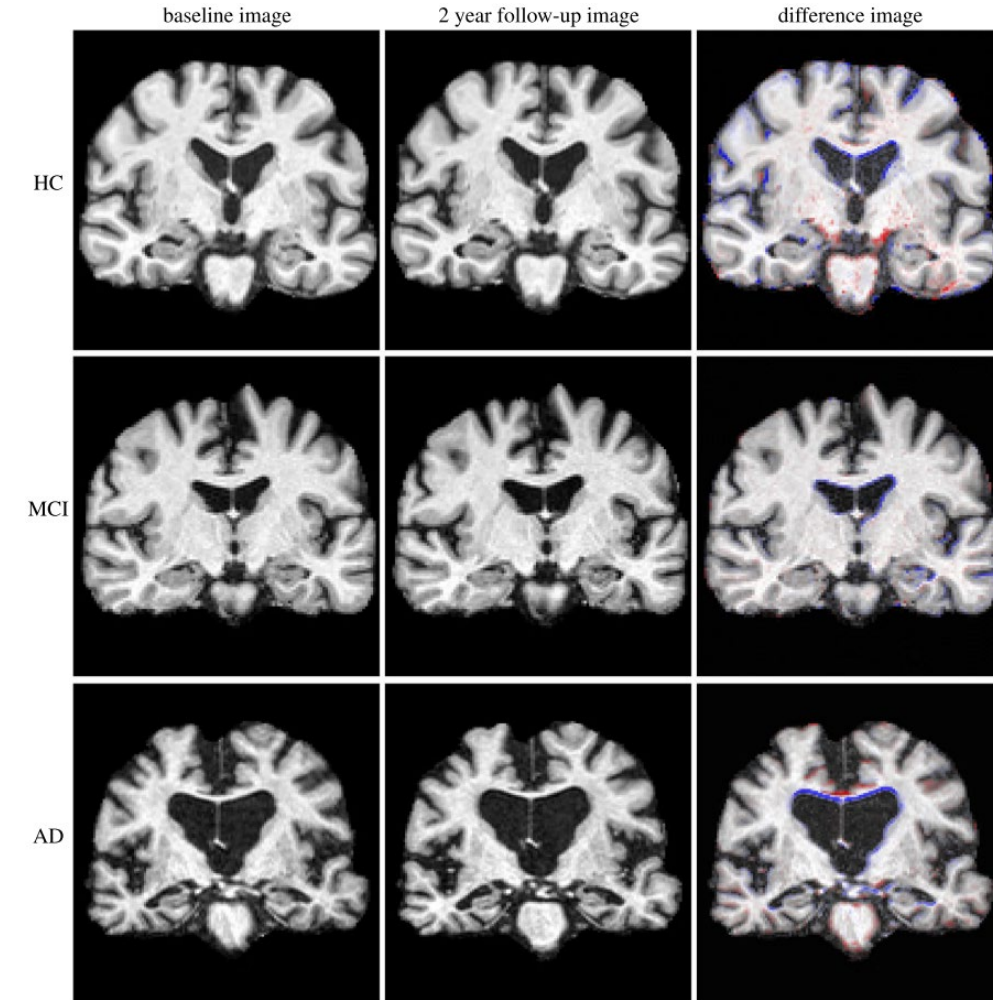
Fig. 1. Regions of the brain regularly observed to decrease their activity during attention demanding cognitive tasks. These data represent a metaanalysis of nine functional brain imaging studies performed with PET and analyzed by Shulman and colleagues.

Raichle, Marcus E., et al. "A default mode of brain function." PNAS 98.2 (2001): 676-682.

FC changes may be also found with MRI and PET

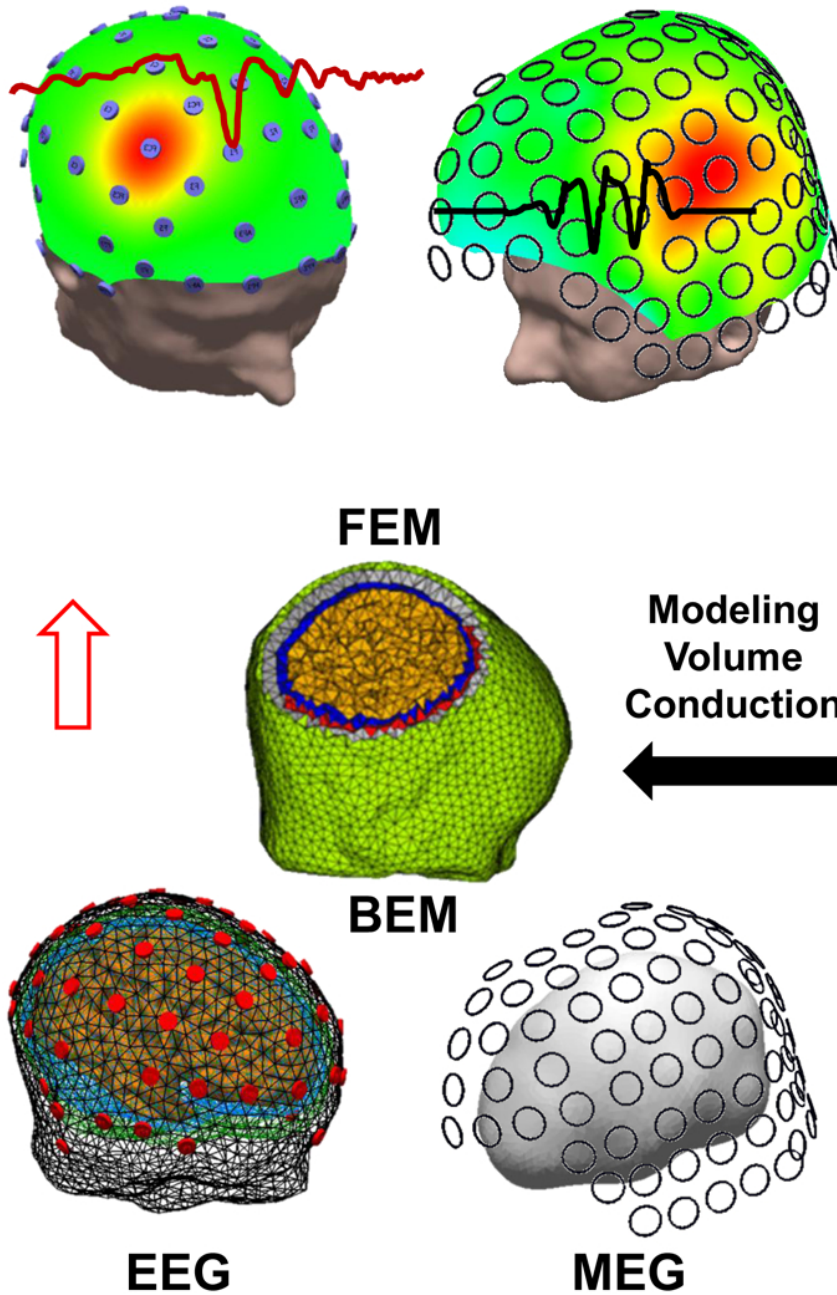


Top row: a healthy control subject (male, 84.8 years at baseline); **Middle row:** MCI subject (female, 71.8 year at baseline) who converted to AD after three years; **Bottom row:** an AD patient (male, 77.5 years at baseline); **Left column:** baseline; **Middle column:** 2-year follow-up; **Right column:** baseline with overlaid difference image of rigidly aligned images (**blue**: volume loss/atrophy, **red**: positive volume change);



Functional connectivity with EEG/MEG

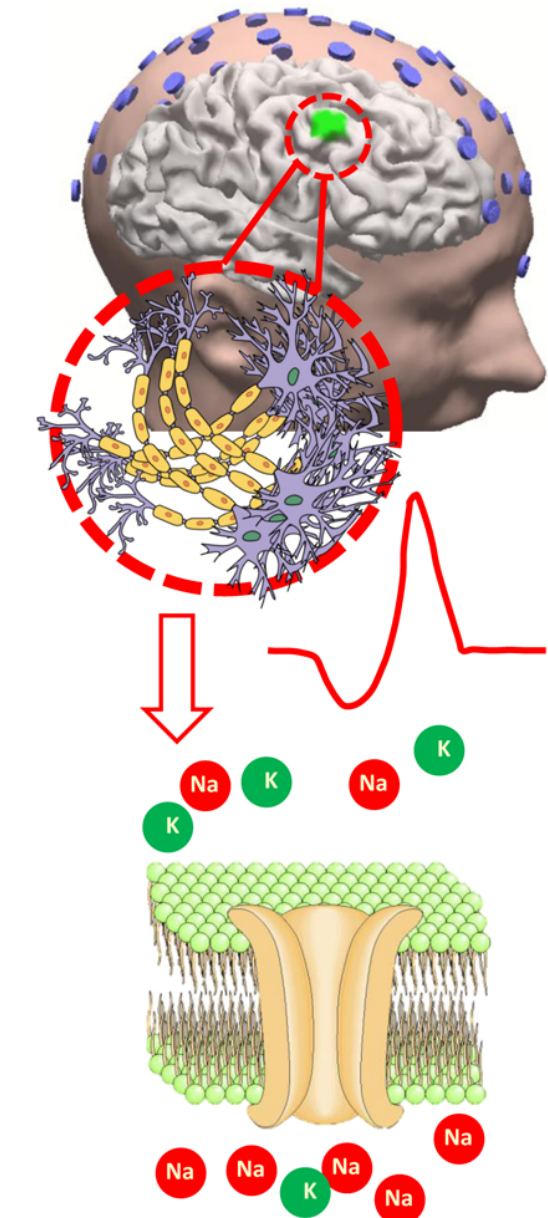
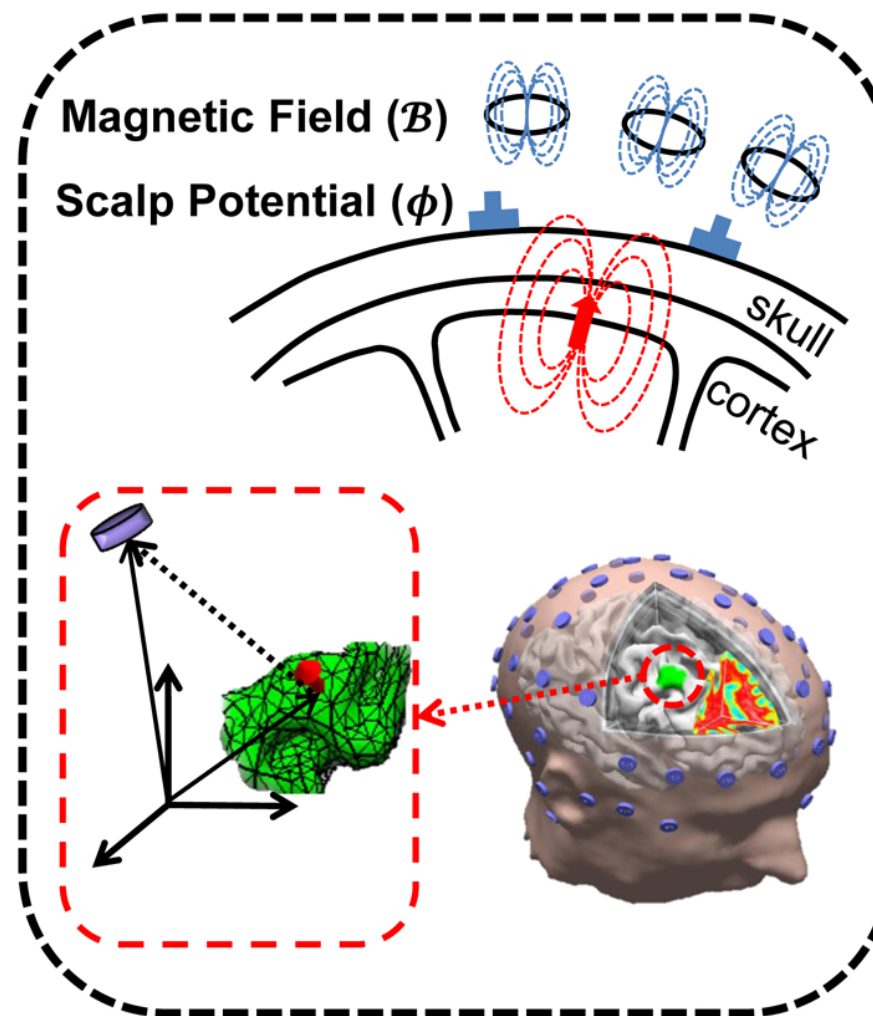
EEG / MEG Measurements



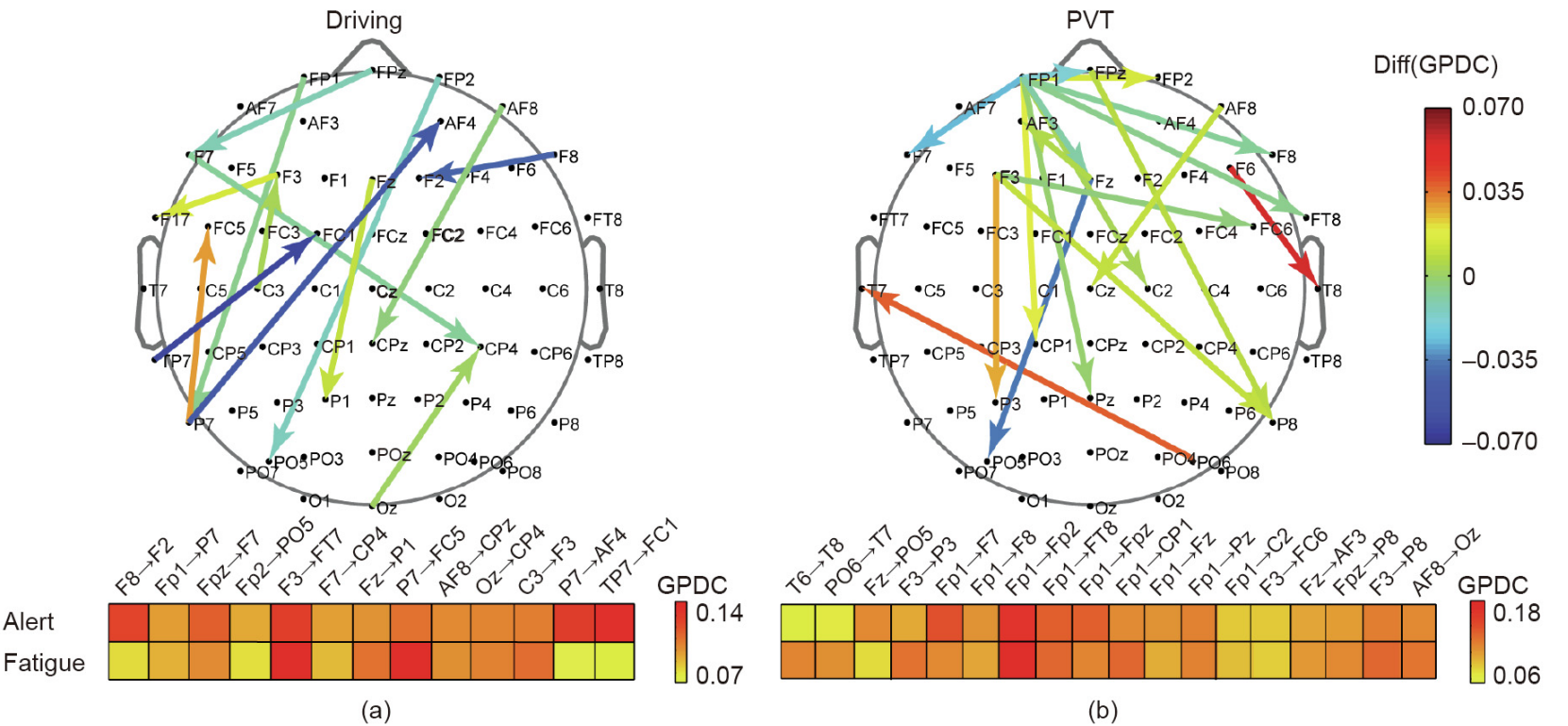
Forward Problem

$$\phi / \mathcal{B} = \mathcal{K} j + n$$

Inverse Problem

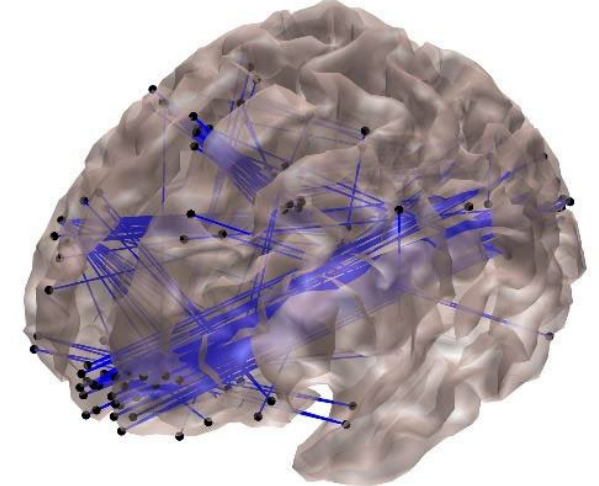


Sensor-based vs source FC analysis of EEG/MEG data

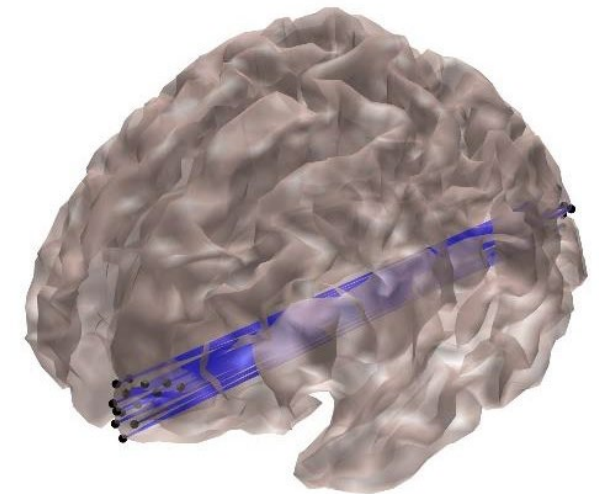


Qi, Peng, et al. "Neural mechanisms of mental fatigue revisited: New insights from the brain connectome." *Engineering* 5.2 (2019): 276-286

A) Selected FC: $p < 10^{-6}$

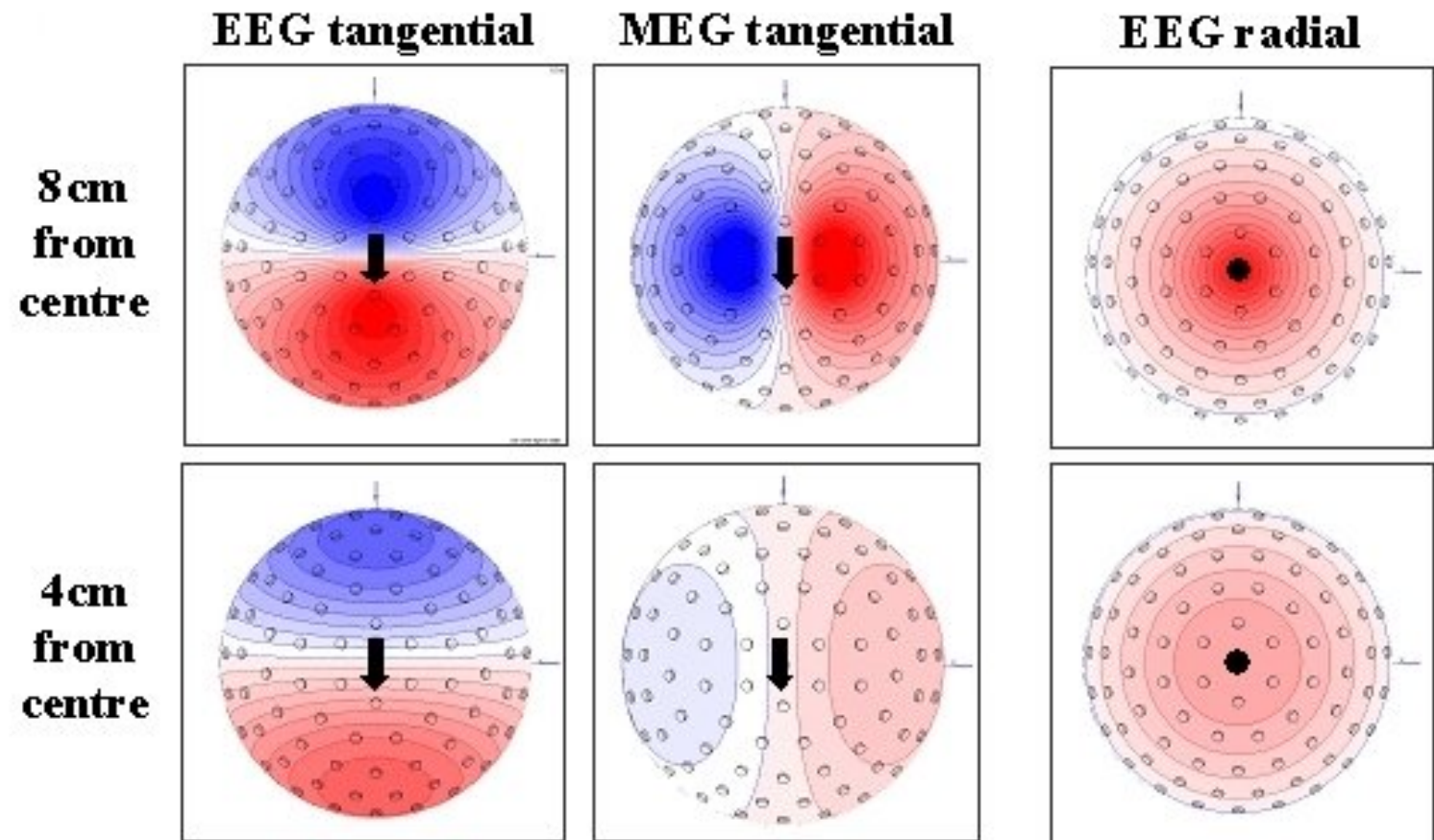
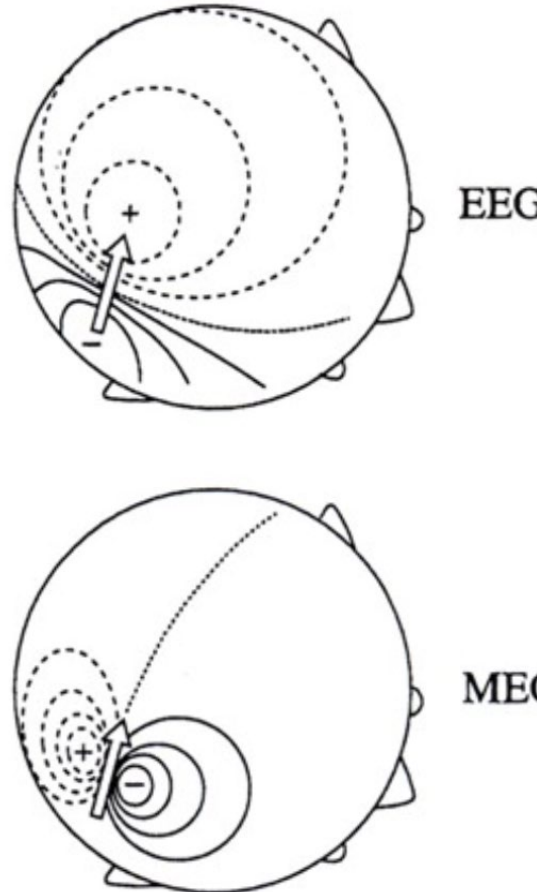


B) Significant FC cluster

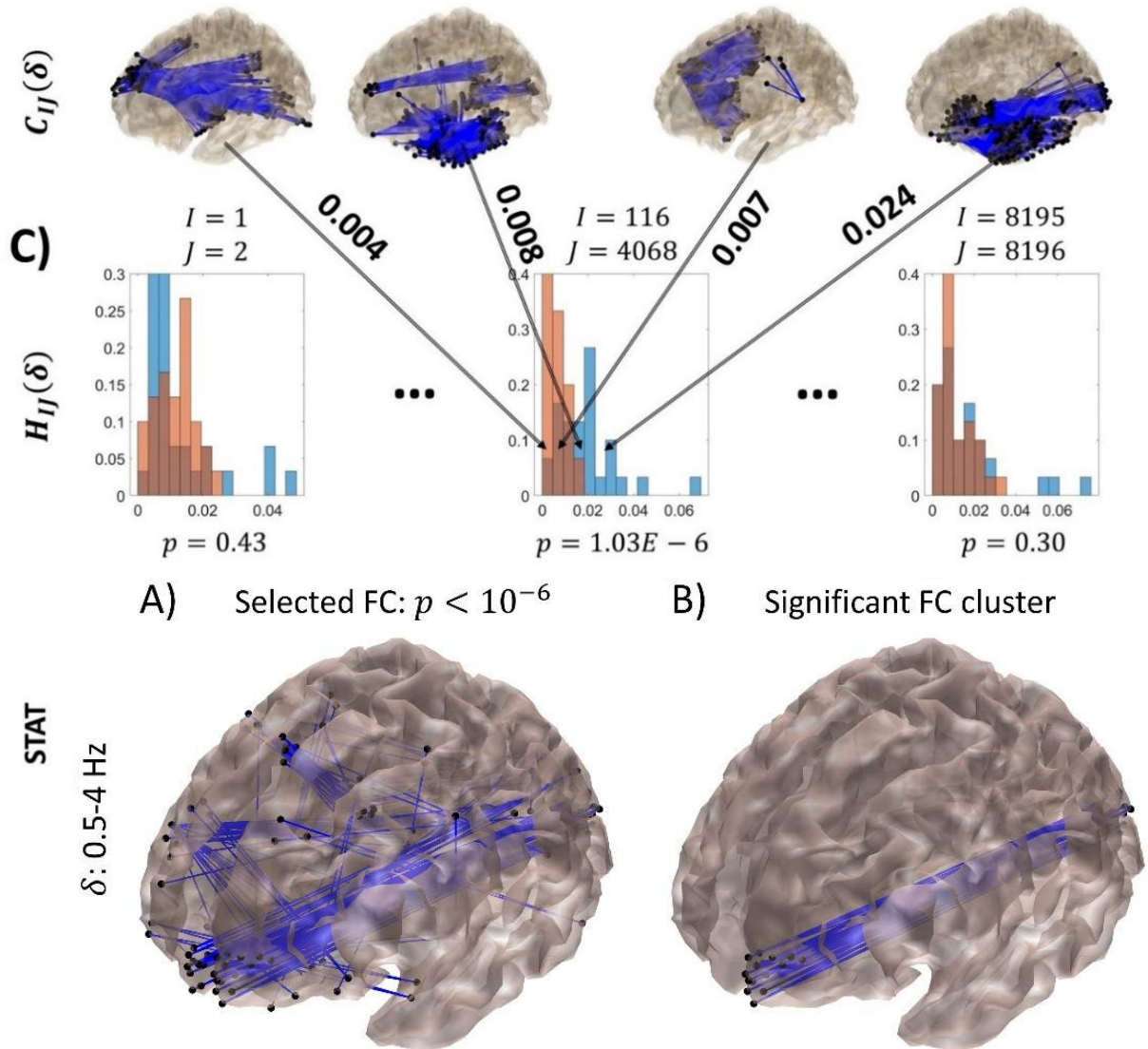
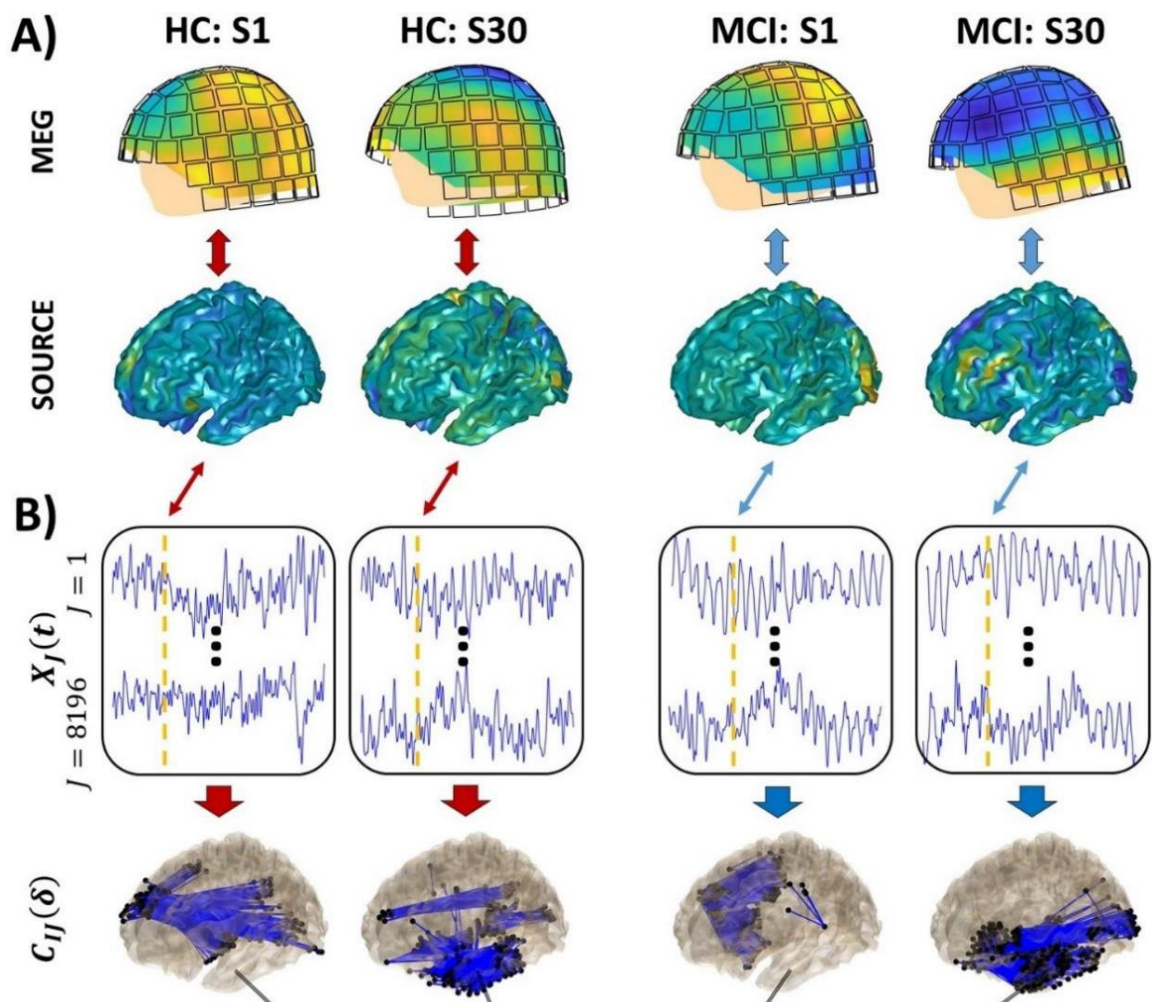


Sanchez-Bornot, Jose M., et al. "High-dimensional brain-wide functional connectivity mapping in magnetoencephalography." *Journal of Neuroscience Methods* 348 (2021): 108991

The nature of the signal, as well as the location of the dipole, have influence in the sensor spatial patterns



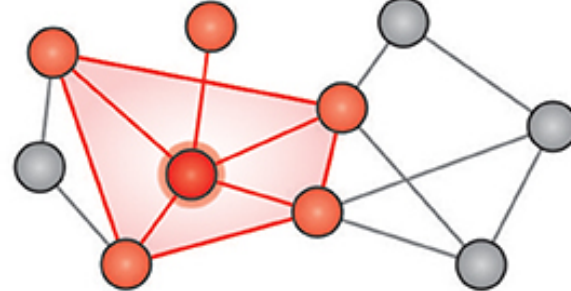
Pipeline for the FC analysis in the source space



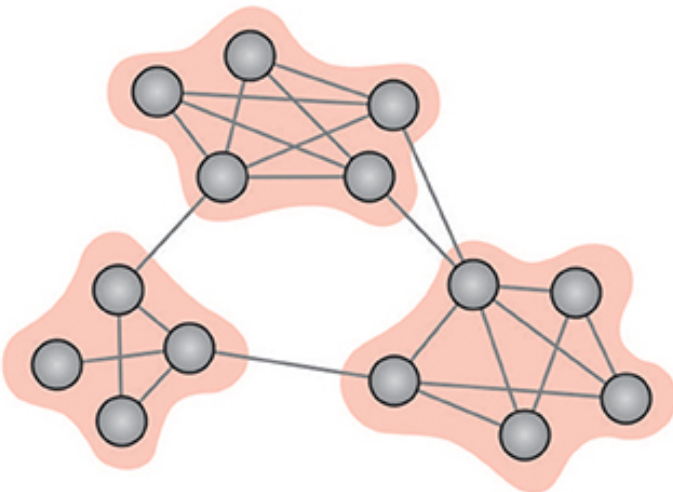


A

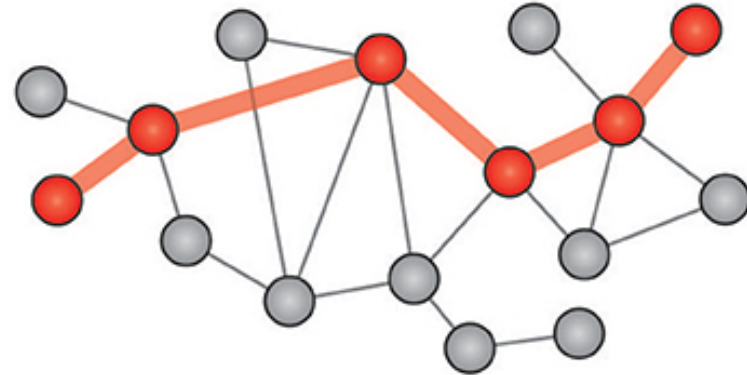
Clustering coefficient



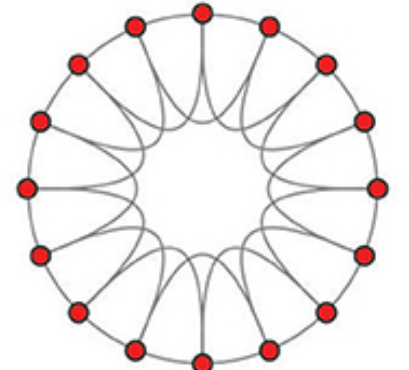
Modularity

**B**

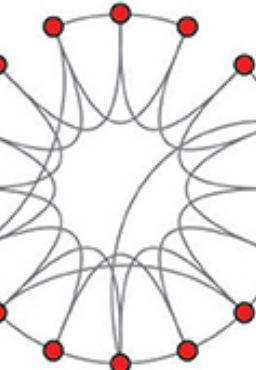
Shortest path

**C**

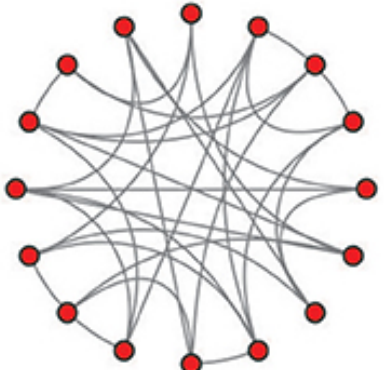
Regular



Small-World



Random

 $\rho = 0$

→ Increasing randomness → $\rho = 1$

D

Assortative



Disassortative



